Testing the survival of microfossils in artificial martian sedimentary meteorites during entry into Earth's atmosphere: the STONE 6 experiment

Frédéric Foucher, Francès Westall, Franz Brandstätter, René Demets, John Parnell, Charles S. Cockell, Howell G.M. Edwards, Jean-Michel Bény, André Brack

Testing the survival of microfossils in artificial martian sedimentary meteorites during entry into Earth's atmosphere: The STONE 6 experiment

Frédéric Foucher[a1]
Frances Westall[a1]
Franz Brandstätter[b2]
René Demets[c, 3]
John Parnell[d,4]
Charles S. Cockell[e5]
Howell G.M. Edwards[f,6]
Jean-Michel Bény[g, 7]
André Brack[a,1]

- [a] Centre de Biophysique Moléculaire, UPR CNRS 4301, 45071 Orléans cedex 2, France
- [b] Naturhistorisches Museum, Min.-Pet. Abteilung, Burgring 7, 1010 Wien, Austria
- [c] European Space & Technology Centre (ESTEC), Keplerlaan 1, Postbus 299, 2200 AG Noordwijk, The Netherlands
- [d] Geofluids Research Group, Dept. of Geology & Petroleum Geology, University of Aberdeen, King's College, Aberdeen AB24 3UE, United Kingdom
- [e] Geomicrobiology Research Group, CEPSAR, Open University, Milton Keynes MK7 6AA, United Kingdom
- [f] Chemical and Forensic Sciences, School of Life Sciences, University of Bradford, Bradford BD7 1DP, United Kingdom
- [g] Institut des Sciences de la Terre d'Orléans (ISTO), UMR CNRS 6113, 1A, rue de la Férollerie, 45071 Orléans cedex 2, France

Abstract

If life ever appeared on Mars, could we find traces of primitive life embedded in sedimentary meteorites? To answer this question, a 3.5-byr-old volcanic sediment containing microfossils was embedded in the heat shield of a space capsule in order to test survival of the rock and the microfossils during entry into the Earth's atmosphere (the STONE 6 experiment). The silicified volcanic sediment from the Kitty's Gap Chert (Pilbara, Australia) is considered to be an excellent analogue for Noachian-age volcanic sediments. The microfossils in the chert are also analogues for potential martian life. An additional goal was to investigate the survival of living microorganisms (*Chroococcidiopsis*) protected by a 2-cm thick layer of rock in order to test whether living endolithic organisms could survive atmospheric entry when protected by a rocky coating.

Mineralogical alteration of the sediment due to shock heating was manifested by the formation of a fusion crust, cracks in the chert due to prograde and retrograde changes of α quartz to β quartz, increase in the size of the fluid inclusions, and dewatering of the hydromuscovite-replaced volcanic protoliths. The carbonaceous microfossils embedded in the chert matrix survived in the rock away from the fusion crust but there was an increase in the maturity index of the kerogen towards the crust. We conclude that this kind of sediment can survive atmospheric entry and, if it contains microfossils, they could also survive. The living microorganisms were, however, completely carbonised by flame leakage to the back of the

sample and therefore non-viable. However, using an analytical model to estimate the temperature reached within the sample thickness, we conclude that, even without flame leakage, the living organisms probably need to be protected by at least 5 cm of rock in order to be shielded from the intense heat of entry.

Keywords

1. Introduction

1.1. Research into the oldest traces of life

Research into the origin of life and the most ancient traces of life is hampered by the fact that suitable rocks dating back to the first billion years of Earth's history are lacking due to alteration by metamorphism and destruction by plate tectonics. The oldest known sedimentary rocks in the Isua Greenstone Belt and on Akilia island, in south-western Greenland (3.85–3.7 Ga, Nutman et al., 1997 and Blichert-Toft et al., 1999) consist of cherts (i.e. silicified volcanic silts and sands), banded iron formation (BIF) and minor strata such as conglomerates (Fedo and Whitehouse, 2002), although the amphibolite to granulite-grade metamorphism makes interpretation of the sedimentary protoliths difficult (Mojzsis et al., 1996, Rosing, 1999, van Zuilen et al., 2002 and Westall and Folk, 2003). The oldest unambiguous traces of life occur in 3.5–3.3-Ga-old Early Archean silicified sediments (cherts) from the Pilbara (Australia) and Barberton (South Africa) greenstone belts. The cherts contain a variety of traces of life, including colonies of small coccoidal chemo(litho)trophic microorganisms on volcanic rock/particle surfaces (Furnes et al., 2004 and Westall et al., 2006) and anoxygenic photosynthetic mats formed in sub-aerial shallow water environments (Allwood et al., 2006, Allwood et al., 2009, Walsh, 2004, Westall et al., 2006 and Tice and Lowe, 2004). From the relatively advanced level of evolution of these microorganisms Westall and Southam (2006) concluded that life had to have appeared much earlier, before ≈4.0 Ga. The presence of microorganisms in shallow water to littoral environments shows that the relatively inhospitable conditions on the primitive Earth (high flux of UV radiation, moderate to relatively high seawater temperatures, high seawater salinity, anoxygenic atmosphere, meteorite bombardment, etc.) did not inhibit life.

The presence of liquid water on Mars during the Noachian period (−4.5 to −3.5 Ga) is now well established (Bibring et al., 2005 and Carr, 2006) and the hydrological system of Noachian Mars as been described by Fassett and Head (2008). Environmental conditions on early Mars during this period were habitable and, in some respects, similar to those existing on the primitive Earth (presence of liquid water, moderate to relatively high water temperatures in the vicinity of hydrothermal vents and volcanic activity, probably high salinity, probably slightly acidic pH due to the CO_2 atmosphere, high flux of UV radiation, meteorite bombardment, etc.) (Westall, 2005). Since Mars had the same ingredients for life (liquid water in contact with mineral surfaces, carbon and other essential elements, and sources of energy), it is widely believed that life could have appeared on that planet (Brack, 1996, McKay, 2008, Sephton and Botta, 2008, Southam et al., 2007, Southam and Westall,

2007, Walter and des Marais, 1993 and Wentworth et al., 2005). Given the lack of terrestrial rocks old enough to contain traces of the first living cells, the discovery of traces of primitive life in ancient rocks on Mars would help understand the origin of life in general (Brack, 1997, Brack et al., 1999 and Westall et al., 2000).

Present and future martian missions are dedicated to studies of the habitable potential of the martian surface (rocks and regolith), as well as to the search for past and present traces of life. The lander Phoenix looked for water on the surface of Mars and tried to determine if life could still exist in the surface materials (Renno et al., 2009). However, the probability of finding living microorganisms in the uppermost centimetres of regolith is very small. Nevertheless, one of our goals was to test the hypothesis that living endolithic organisms (i.e. microorganisms that live within rocks) could survive ejection from the host planet, transport through space, and entry into the atmosphere of another planet, such as Earth. With this objective in mind, we subjected living endolithic organisms, *Chroococcidiopsis*, protected by a 2-cm thick layer of rock to the heat shock of entry into the Earth's atmosphere.

Other missions to Mars will investigate the habitability of the surface (the NASA-led Mars Science Laboratory (MSL), named Curiosity, 2011 mission) and search for traces of present or past life (the ESA led 2018 ExoMars mission). The search for traces of life *in situ* promises to be challenging since it is already difficult to unambiguously identify traces of fossil life in ≈3.5-Ga-old terrestrial rocks, even with the availability of highly sophisticated instrumentation capable of high resolution observation and analysis. Thus, the most promising method of studying martian materials to detect traces of life will be the international Mars Sample Return mission planned for 2023 (The MEPAG-ND-SAG, 2008).

An alternative method of searching for traces of martian microbial remains (if life appeared on Mars) is to analyse sedimentary meteorites. This solution has two advantages: it is cheaper than space exploration and very accurate analyses can be made in the laboratory. The SNC (Shergottite, Nakhlite, Chassignite) meteorites form a small group of rare meteorites originating from Mars. All the known 52 SNC meteorites so far found[8] consist of igneous rocks, mainly basaltic, that are *a priori* incompatible with the presence of biogenic remains (except as endoliths). However, sediments deposited in bodies of standing water would constitute suitable materials for hosting traces of life. The STONE 6 experiment was therefore carried out in order to test the survival of martian analogue sediments and microfossils embedded in the sediments during entry into the Earth's atmosphere. The survival of living endolithic microorganisms was also investigated.

1.2. STONE experiments

STONE 6 is the latest in a series of experiments whose objectives are to test the effect of entry into the Earth's atmosphere on different sedimentary meteorite analogues (Brack et al., 2002). The rock samples are fixed around the stagnation point of the heat shield of spherical FOTON capsules, 2250 kg in weight and 2.3 m in diameter, used to carry out experiments in lower Earth orbit.

Previous successful STONE experiments include the STONE 1 experiment which tested a carbonate (dolostone, i.e. dolomite, fossil calcareous shells, quartz and feldspar), and an artificial sediment composed of basalt (80%) and gypsum (20%), and a reference sample of dolerite (a variety of basalt) (Brack et al., 2002). Only the dolostone survived. Although it did not exhibit a fusion crust, its composition changed due to high temperature processes; the

carbonate decomposed into CaO and MgO (periclase). All the samples in the 2005 STONE 5 experiment, dolerite, carbonate cemented sandstone, and gneissic impactite, survived atmospheric entry (Brandstätter et al., 2008 and Parnell et al., 2008). A fusion crust formed on the dolerite suggesting that the temperatures attained at the heat shield of the capsule were comparable to those experienced by meteoroids. This STONE experiment also tested the survival of living bacterial and fungal spores, as well as dried vegetative endoliths that were placed in tiny wells drilled into the 1-cm thick rock discs. However, the shield constituted by the rocks (1 cm) was too thin and the microorganisms were carbonised during atmospheric entry (Cockell et al., 2007). Since endolithic photosynthesising microorganisms require cannot live at great depths within a rock, it is unlikely that they could have been imported from another planet, therefore Cockell et al. (2007) concluded that photosynthesis had to have evolved on Earth.

Our experiment, STONE 6, tested the effect of the atmospheric entry on three samples, the reference sample of dolerite and two sedimentary rocks samples. The latter included Devonian lake sediments ≈400-Myr-old from the Orkney Islands, Scotland and a ≈3.5-byr-old volcanic sandstone, the Kitty's Gap Chert, from the Pilbara region of Australia. This paper concentrates on the observations and analysis carried out on the latter sample. [A second experiment that flew on the same mission, *Lithopanspermia*, consisted of a rock coated with fungal species and is not part of our experiment, de la Torre et al., 2010.]

2. Materials and methods

2.1. The Kitty's Gap Chert

The 3.446-Ga-old Kitty's Gap Chert (Fig. 1) forms part of the Coppin Gap Greenstone Belt, in the Pilbara, north-western Australia. It consists of layers of silicified volcanic silts and sands deposited in an intertidal environment (Westall et al., 2006 and de Vries et al., 2006). The volcanic precursors consisted of K-feldspars, Ti-bearing biotites, volcanic glass shards, amphiboles, and ghost spherulites that were replaced by K-phyllosilicates (hydromuscovite, $KAl_2[(OH, F)_2/AlSi_3O_{10}]–H_2O$) (Orberger et al., 2006). Early diagenetic silicification of the volcaniclastic sediments was due to silica-rich hydrothermal fluids as well as silica-saturated seawater (van den Boorn et al., 2007). The rock was subjected to regional low grade metamorphism (prehnite–pumpellyite grade, Westall et al., 2006). Westall et al. (2006) documented traces of primitive small, anaerobic fossil microorganisms in these sediments, including silicified biofilms and colonies of coccoidal, rod-shaped, filamentous microorganisms. Although remnants of photosynthetic mats (photosynthesis is a relatively advanced metabolism) occur in the sediments, the majority of the microorganisms were probably lithotrophic (a very early metabolism), obtaining their carbon and energy from inorganic sources, in this case the rock/mineral surfaces. The carbonaceous microfossils are well preserved owing to their precocious silicification and the low grade metamorphism of the rocks, although the carbon in the microfossils is thermally mature as is to be expected in rocks of this age and metamorphic grade.
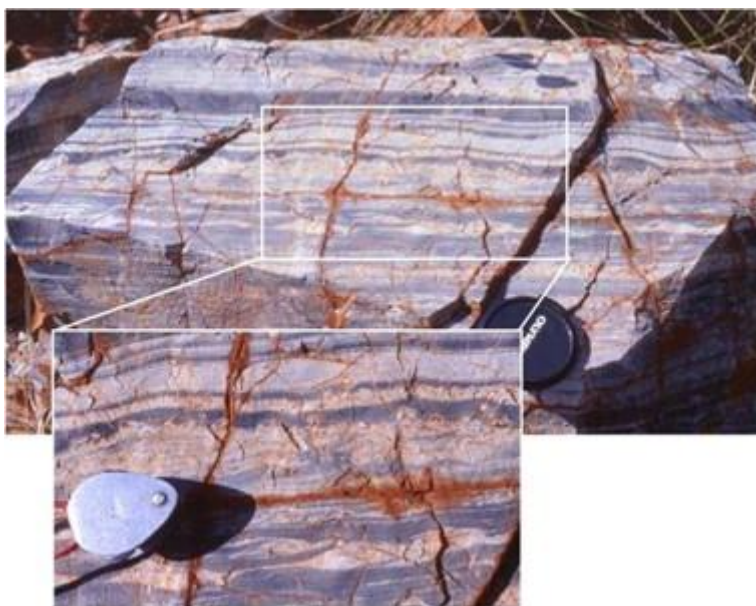
Fig. 1. Field view of the original rock from the Kitty's Gap Chert, Pilbara, Australia.

The shallow water volcanic environmental setting of the Kitty's Gap Chert is one that could have existed on Noachian Mars (Westall, 2005, Fassett and Head, 2008 and Greenwood and Blake, 2004), as demonstrated by recent orbital and *in situ* geochemical studies (Poulet et al., 2005, Bibring et al., 2005, Squyres et al., 2004, Squyres et al., 2008, Bishop et al., 2008 and Milliken et al., 2008). These sediments were, moreover, deposited in an epoch (or soon after) when Mars could have hosted life at its surface (Westall, 2005 and Southam and Westall, 2007). The primitive chemo(litho)trophic organisms that lived on the Early Archean Earth could have inhabited the Noachian martian surface. For this reason, the small, primitive cells that characterise the Kitty's Gap sediments can be considered as analogies for putative early martian microorganisms. The sediments with their fossilised microorganisms therefore constitute useful analogues for martian rocks of Noachian age.

2.2. Sample preparation before launch

In the previous STONE experiments, the rocks were cut into discs 7 cm diameter and 1 cm thickness. One of the objectives of the STONE 6 mission was to test one aspect of the hypothesis of panspermia by evaluating the survival of microbial spores protected by the thickness of the samples. The STONE 5 experiment demonstrated that 1 cm of rock (cut as flat discs) was not sufficient and it was thus decided to increase the thickness. For practical reasons, the samples being now thicker than the sample holders, the rocks were milled into a flanged dome shape that was 2 cm thick at its apex in order to provide more protection for the living microorganisms. The 3.5-Ga-old Kitty's Gap Chert was, however, too fractured to be able to be cut into the required shape and was therefore crushed into ≈3-mm sized fragments and mixed with space-qualified cement (*Sauereisen Electrotemp cement No. 8*) before being poured into a mould of the required form. The space cement is a magnesium phosphate (aMgH$_x$(PO$_y$)$_z$·bH$_2$O) in a zircon (ZrSiO$_4$) and silica (SiO$_2$) base. The final shape of the sample after machining before its fixation on the capsule is shown in Fig. 2. The sample holder consists of an annular disk of phenolic silica, i.e. the same material used for the ablative capsule heat shield. The exposed part of the sample was 5 cm in diameter. The holder was fixed onto the FOTON-M3 capsule near the stagnation point by carbon–carbon screws.
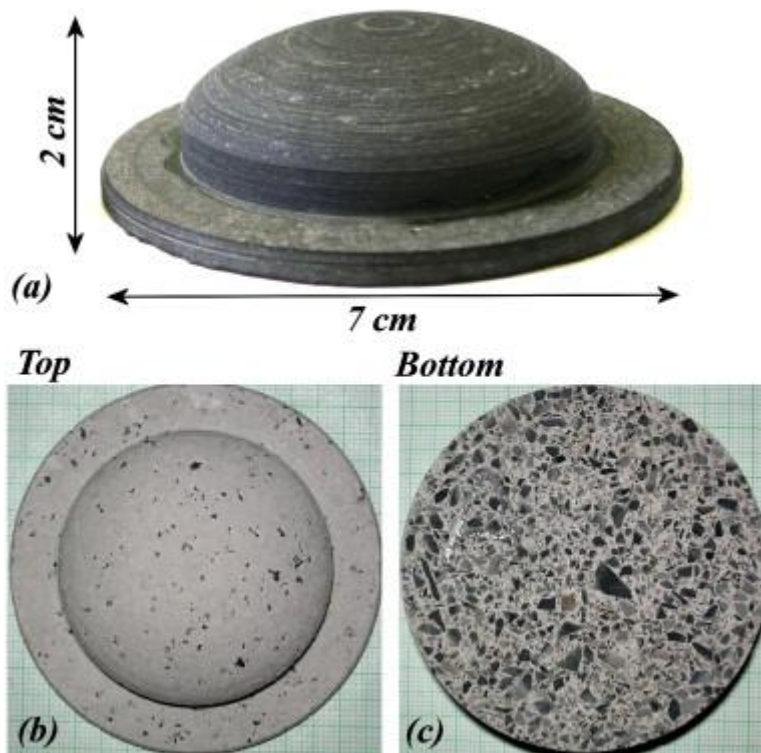
Fig. 2. Final shape of the reconstituted sample consisting of 3-mm sized fragments of chert mixed in space cement (a); top (b) and bottom (c) views of the Kitty's Gap Chert sample. The fragments of the original rock mixed in cement are clearly visible.

A live, hydrated culture of the photosynthetic endolithic microorganism, *Chroococcidiopsis*, was painted on the back of the rock before it was screwed into the sample holder.

2.3. Flight details

The FOTON-M3 capsule was launched by a Soyuz-U launcher rocket from Baikonur (Kazakhstan) on 14 September 2007. On the 26th September after 12 days in lower Earth orbit, the velocity of the capsule was slightly decreased from 7.7 km/s to 7.6 km/s for atmospheric entry. The re-entry module underwent thermal shock as it entered the stratosphere. Mineralogical changes detailed below show that the temperature on the ablation surface started from a few degree Celcius, increased up to 2000 °C at the apex and decreased to less than 0 °C within a few tens of seconds. The speed of the capsule was reduced by parachute and brake rocket for landing in a field in Kazakhstan.

Two of the three STONE samples survived the experiment, as did the *Lithopanspermia* sample; the reference dolerite sample was lost. A photograph of the capsule after landing is shown in Fig. 3. The Kitty's Gap Chert sample exhibited a bright white fusion crust across the entire exposed surface (see inset in Fig. 3). The final thickness of the sample ranged from 9 to 10 mm, corresponding to a loss of ≈50% of the initial thickness by ablation.

Fig. 3. FOTON-M3 capsule after landing showing emplacement of the rock sample around the stagnation point. Detail of the Kitty's Gap Chert sample, showing the presence of a white fusion crust over the whole of the exposed surface and streaming of solidified molten rock and heat shield material (inset).

After landing, the samples were carefully and rapidly removed from the capsule in relatively sterile conditions using glove-covered hands and stored in a protective holder (Fig. 4) for transport to a clean room at the European Space & Technology Centre (ESTEC, Noordwijk, The Netherlands), from where they were collected for analysis. The transport containers had been specifically constructed to protect the samples during transport after the disintegration of one of the rocks (sandstone) used in the STONE 5 experiment.
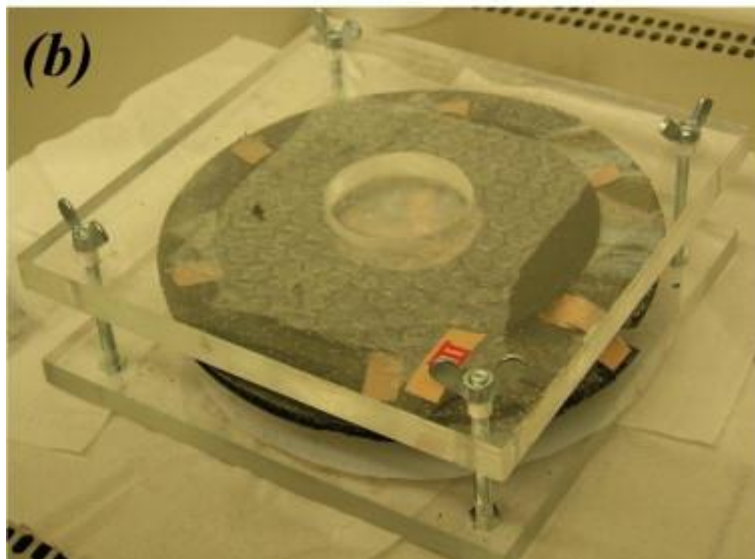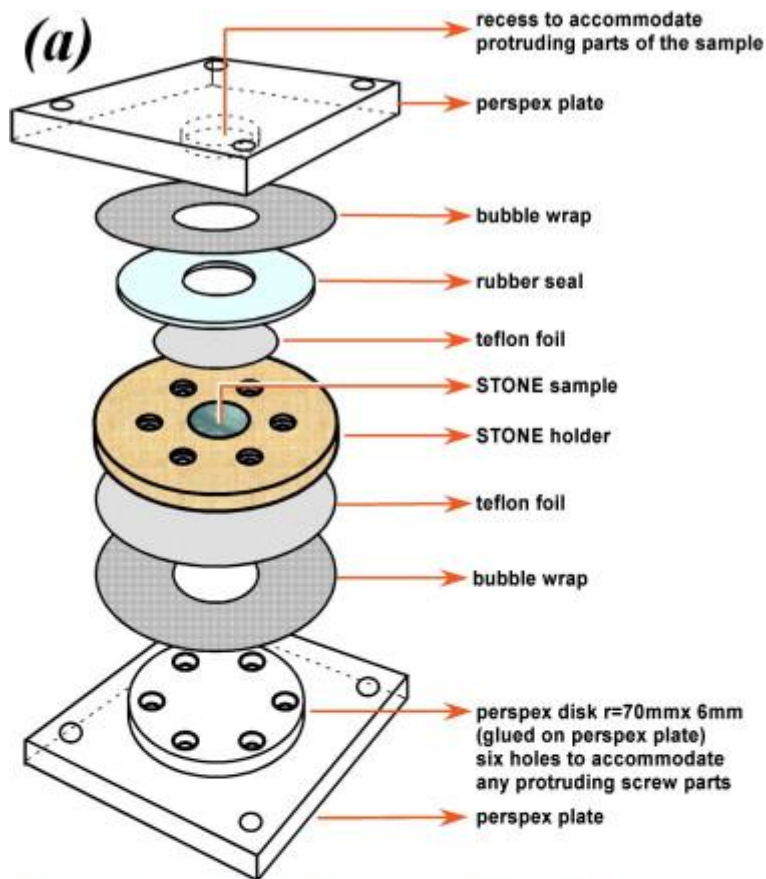
Fig. 4. (a) Sketch of transportation container and (b) photograph of the sample in the container in the clean room at ESA–ESTEC.

2.4. Sample preparation after landing

In order to study changes in the Kitty's Gap Chert fragments through the thickness of the reconstituted rock, 30 μm and 500 μm thick polished sections were prepared (Fig. 5). Some of the sections were etched by hydrofluoric acid (HF) in order to dissolve the chert and to reveal

the embedded organic matter. The method chosen consisted of etching portions of the 500 μm thick sections with HF droplets (24% in concentration) deposited for 45 min, followed by abundant rinsing with *milliQ* water. Slightly etched surfaces of 30 μm thick thin sections were also observed (HF 2.5% and HF 5% during 30 min).
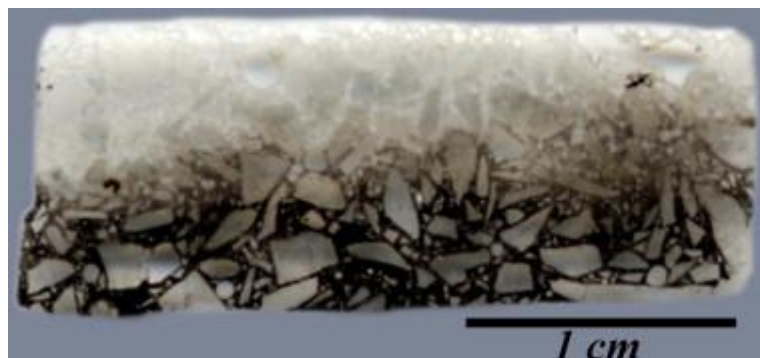

Fig. 5. Polished thin section 30 μm thick of the Kitty's Gap Chert sample after atmospheric re-entry. The fusion crust is at the top, denoted by a thin (<1 mm) bright white layer. Note the dark colour of the cement in the lower part of the image.

2.5. Analytical methods

Several methods were used to observe, analyse and characterise the sample. An optical microscope (Olympus BX51, CBM-Orléans) was used to make preliminary observations and to localize specific areas of interest. Atomic force microscopy (AFM, Veeco D3100, CBM-Orléans) and Scanning Electron Microscopy (FEG SEM, Hitachi S4200, Centre de Microscopie Électronique, Orléans) were used both on etched and un-etched surfaces to make high magnification observations of specific structures. Elemental analyses were made with an Energy Dispersive X-ray spectrometer (EDX) attached to the SEM, as well a Cameca SX 50 microprobe (BRGM-Orléans). Raman spectroscopy was made with a Dilor XY800 (ISTO-Orléans), and WITec Alpha 500RA (CBM-Orléans) to make compositional analysis and to study the changes in the organic matter and in the minerals with reference to distance from the fusion crust.

3. Results

3.1. General optical aspect

The post-flight rock exhibits a flat bright white vitreous surface, in comparison to the matt variegated cream-coloured cupola of the preflown reconstituted rock. The sample is 9–10 mm thick, whereas the preflown rock had a maximum thickness of 20 mm at its apex.

In cross section, the post-flight sample can be divided into three zones parallel to the fusion crust (Fig. 5). The fusion crust itself is ≈0.8 mm thick and characterised by a bright white colour and glassy reflection. The lower ≈5 mm of the sample appears blackened to the naked eye although in thin section it is only the cement that has become black. In between the fusion crust and the lower blackened layer the sample shows a dull creamy white colour. In the

following, mineralogical and morphological changes in the flown rock will be described for each constituent with respect to distance from the exposed surface, labelled x.

3.2. Rock fragments

3.2.1. Chert matrix

3.2.1.1. Pre-flight sample

The original rock consists of volcanic protoliths replaced by hydromuscovite within a microcrystalline ($\leqslant 1$ μm) matrix of α quartz (quartz) that, in places, has been slightly recrystallised into euhedral crystals 5–10 μm in size. Small (≈ 1 μm) and irregular-shaped fluid inclusions occur in the chert matrix of the original rock. Sample preparation for flight produced no mechanical modifications, such as fracturing (*N.B.* the original rock is moderately fractured with the fractures coloured by Fe oxide deposits).

3.2.1.2. Post-flight sample

In the fusion crust (i.e. for $x < 0.8$ mm), the chert fragments are completely fused to a glassy texture in which no volcanic protoliths can be distinguished (Fig. 6b). Several bubbles consisting of trapped air (Raman analyses) are also observed (Fig. 6b), the air being incorporated during rapid cooling of the melted material after atmospheric entry. Broadening of the 465 cm^{-1} peak of quartz in the Raman spectrum (Fig. 6a) taken within the fusion crust indicates that the quartz phase is completely amorphous. As can be observed in the optical micrograph and the Raman map of the 465 cm^{-1} quartz peak (Fig. 6b and c), the transition between the fusion crust and the underlying non-fused sample is relatively sharp with only a narrow band of mixed amorphous and crystalline quartz between 0.7 mm $< x < 0.8$ mm (Fig. 6a). Quartz below 0.8 mm from the sample surface is well preserved (Fig. 6a) although some fractures traverse the chert fragments (Fig. 7a). In this zone fractures in the chert matrix also radiate out from embedded volcanic protolith particles and are commonly lined with bubbles (Fig. 7b). There is no change in the size and shape of the fluid inclusions in the chert in the zone furthest away from the fusion crust but, in the middle of the sample (between 0.8 mm and 3 mm), the H_2O-filled inclusions have rounded shapes and can be up to 50 μm in size.
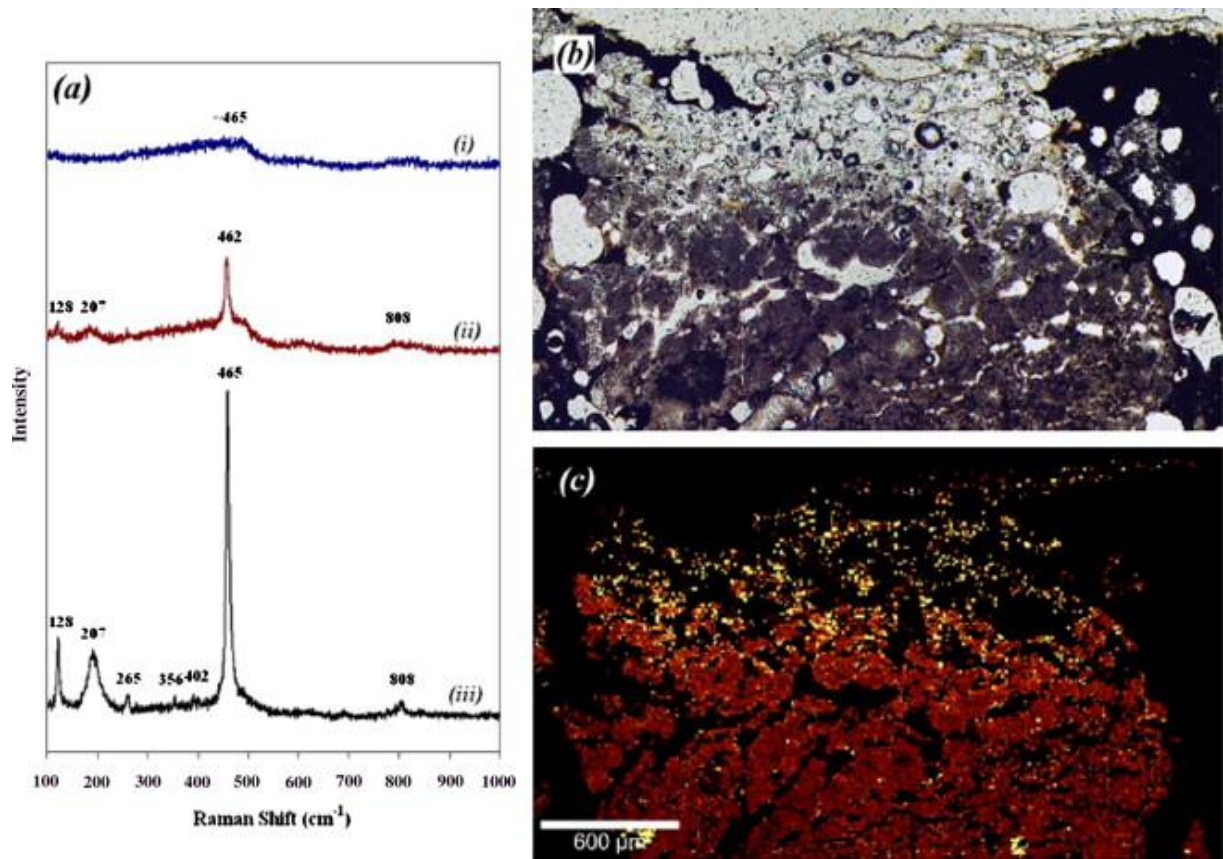
Fig. 6. Analysis of the quartz in the fusion crust. (a) Raman spectra of quartz (i) spectrum at 0.4 mm from the exposed surface (glassy state), (ii) spectrum at 0.7 mm from the exposed surface (mixed state), and (iii) spectrum at 1.2 mm from the exposed surface. (b) The optical image clearly shows the presence of bubbles in the glassy fusion crust. (c) Raman mapping associated with the optical image represents the evolution of the width of the 465 cm^{-1} peak of the quartz, the dark area being associated with well preserved quartz.
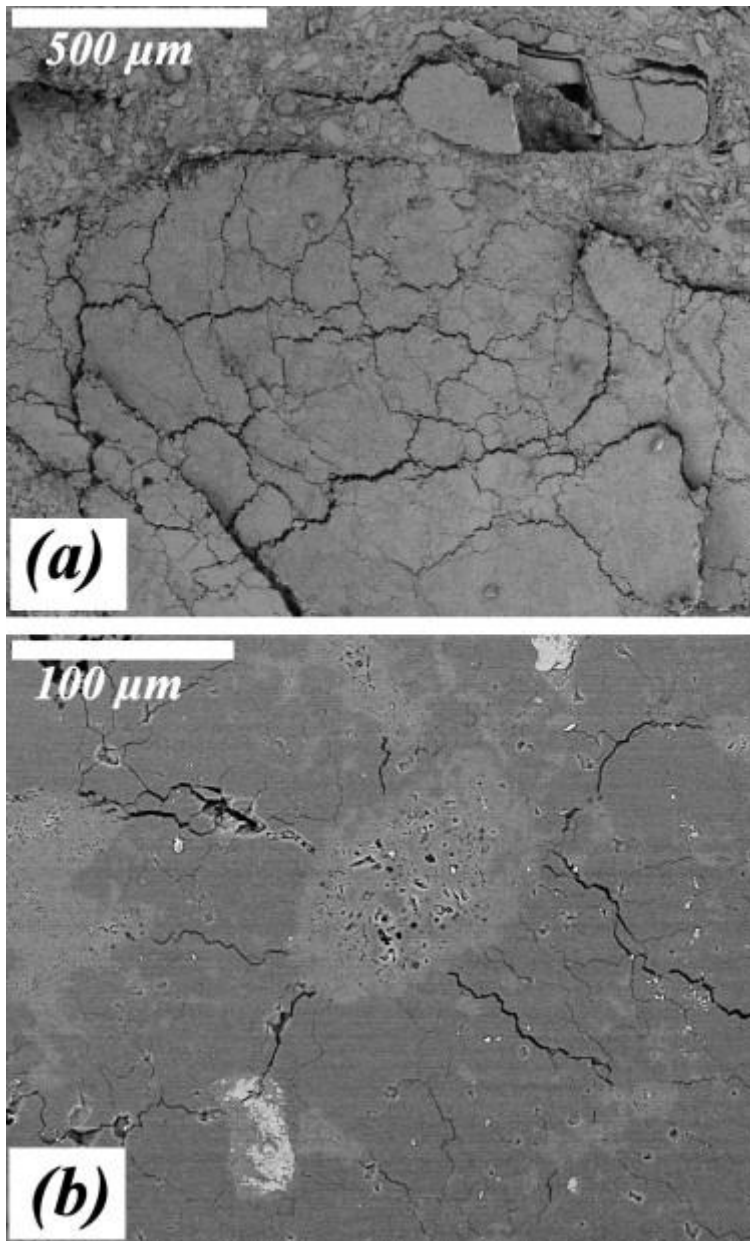
Fig. 7. (a) SEM image of cracks in and around a quartz particle after slight etching (HF 5%, 30 min, distance from the exposed surface 7.6 mm). (b) Hydromuscovite grains after loss of OH, surrounded by cracks in the quartz matrix (distance from the exposed surface 4.6 mm).

3.2.2. Volcanic protoliths

3.2.2.1. Pre-flight sample

The silicified hydromuscovite-replaced volcanic protoliths in the original rock exhibit irregular angular to euhedral shapes, depending on the original composition of the protolith (feldspar, volcanic glass, pyroxene; Orberger et al., 2006). Raman spectra of the hydromuscovite are characterised by a weak but highly fluorescent signal, the weakness of the signal being due to strong silicification of the original rock.

Ti oxides, anatase and rutile, are associated with the volcanic protoliths and are common throughout the sample. Anatase is the dominant phase and occurs in aggregates dispersed throughout the chert fragments, as well as along the edges of the volcanic protoliths. Rutile occurs as tiny (≈1 μm) sparse isolated crystals within the anatase, especially inside the protoliths. Carbon is frequently associated with anatase.

3.2.2.2. Post-flight sample

In the fusion crust (top 0.8 mm) where the chert fragments are glassy, there is no trace of the protoliths due to complete melting of the minerals (Fig. 6b). In the middle of the section (between 0.8 mm and 5 mm), the volcanic protoliths have an inhomogeneous dark appearance (Fig. 8a) compared to their transparent brownish colour at the back of the sample (Fig. 8b). They are characterised by water-filled spherical inclusions (Fig. 9) although the concentration of the inclusions within the hydromuscovite is variable owing to local variations in the degree of silica replacement of the phyllosilicate.
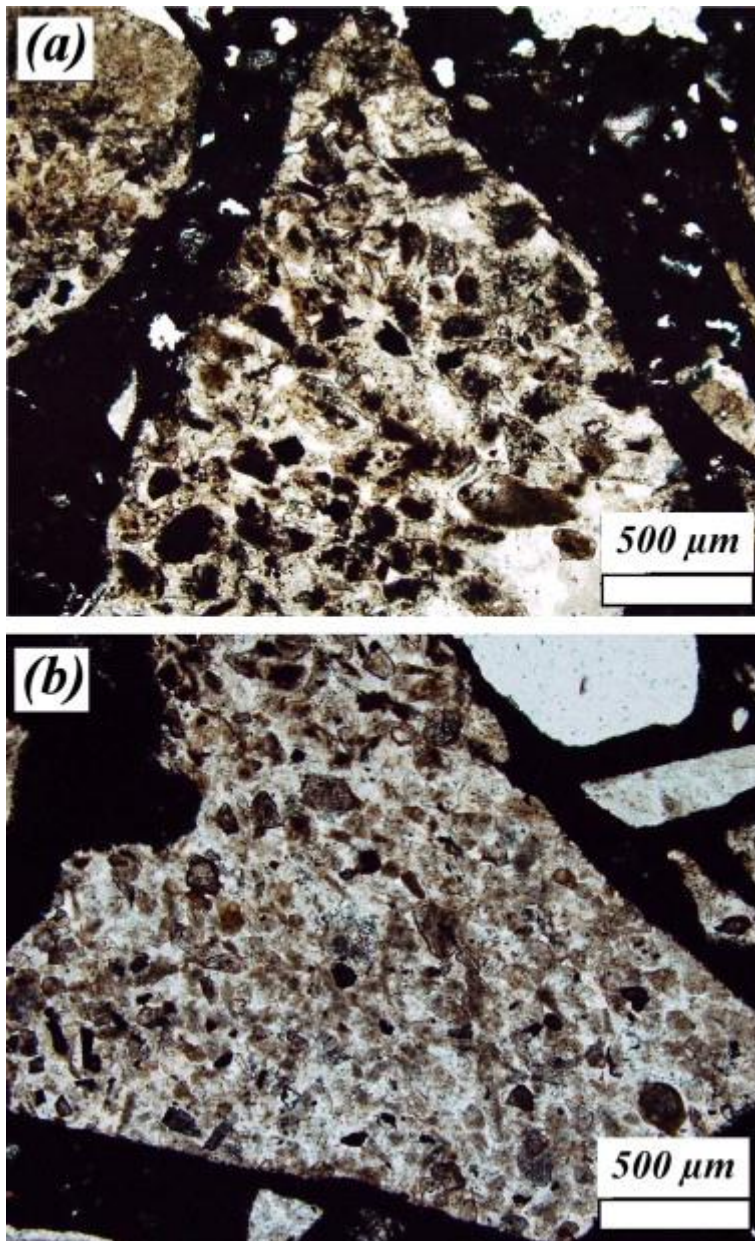
Fig. 8. Optical view of the volcanic protoliths (a) in the middle of the section (distance from the exposed surface 4 mm) with a dark appearance and (b) at the back of the sample (distance from the exposed surface 8 mm).

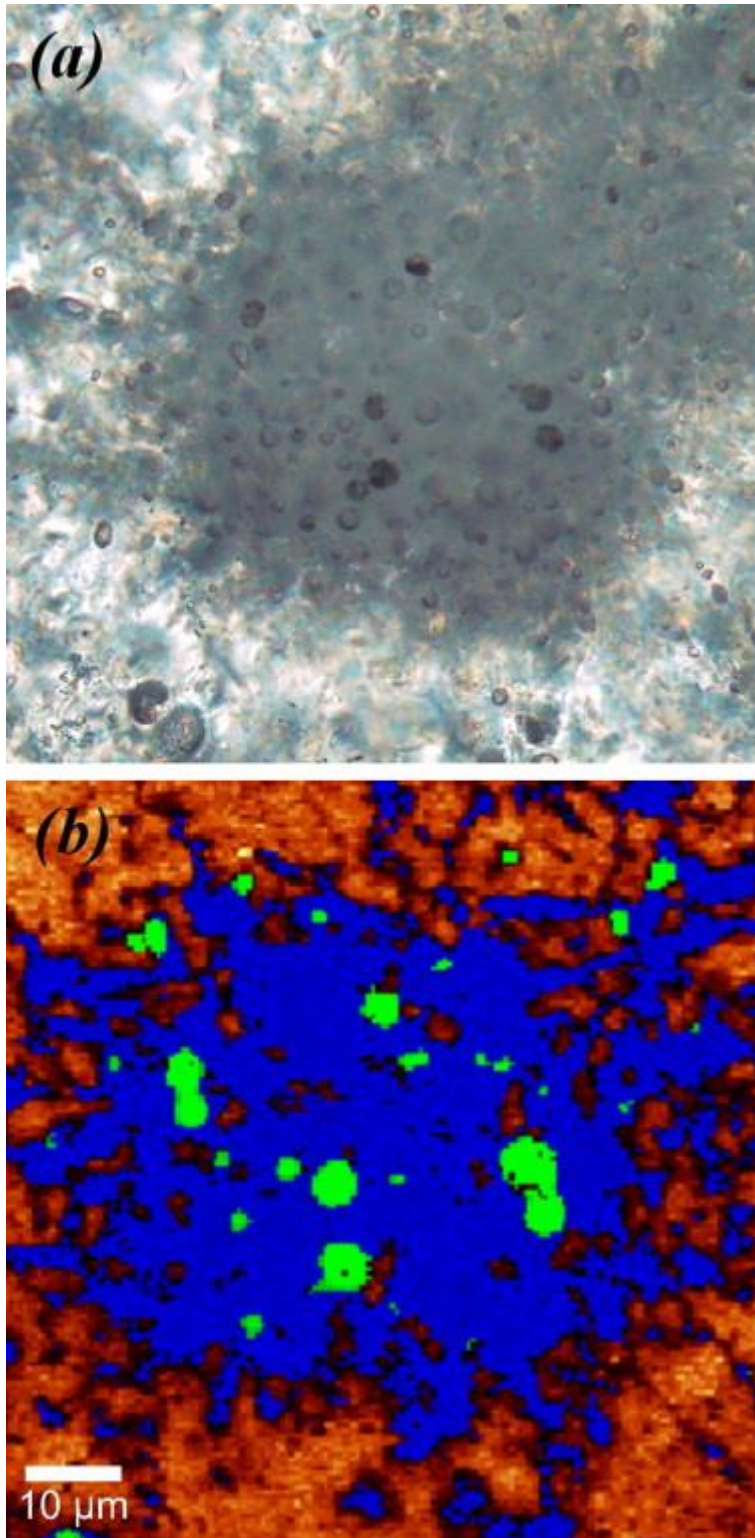Fig. 9. Optical and Raman images of a melted hydromuscovite grain located at 1.9 mm from the exposed surface. The H_2O-filled bubbles are clearly highlighted by Raman spectroscopy (colour coding: brown for quartz, blue for melted hydromuscovite and green for water). (For interpretation of the references to colour in this figure legend, the reader is referred to the web version of this article.)

3.3. Cement

3.3.1. Pre-flight sample

The relatively porous cement has a whitish colour and contains zircon and MgO crystals up to 100 μm in size mixed in a matrix consisting of hydrated magnesium phosphate and silica.

3.3.2. Post-flight sample

The most immediately apparent change in the cement is the dark colouration in the lower ≈5 mm of the flown sample (Fig. 5) and fusion with the chert fragments in the fusion crust (top 0.8 mm) leading to the incorporation of Mg in the fused chert (Fig. 10e). As in the chert fragments, air bubbles occur in the cement in the fusion crust and up to 2 mm away from the sample surface. Fractures occur in the space cement throughout the thickness of the sample and are common around the chert particles.
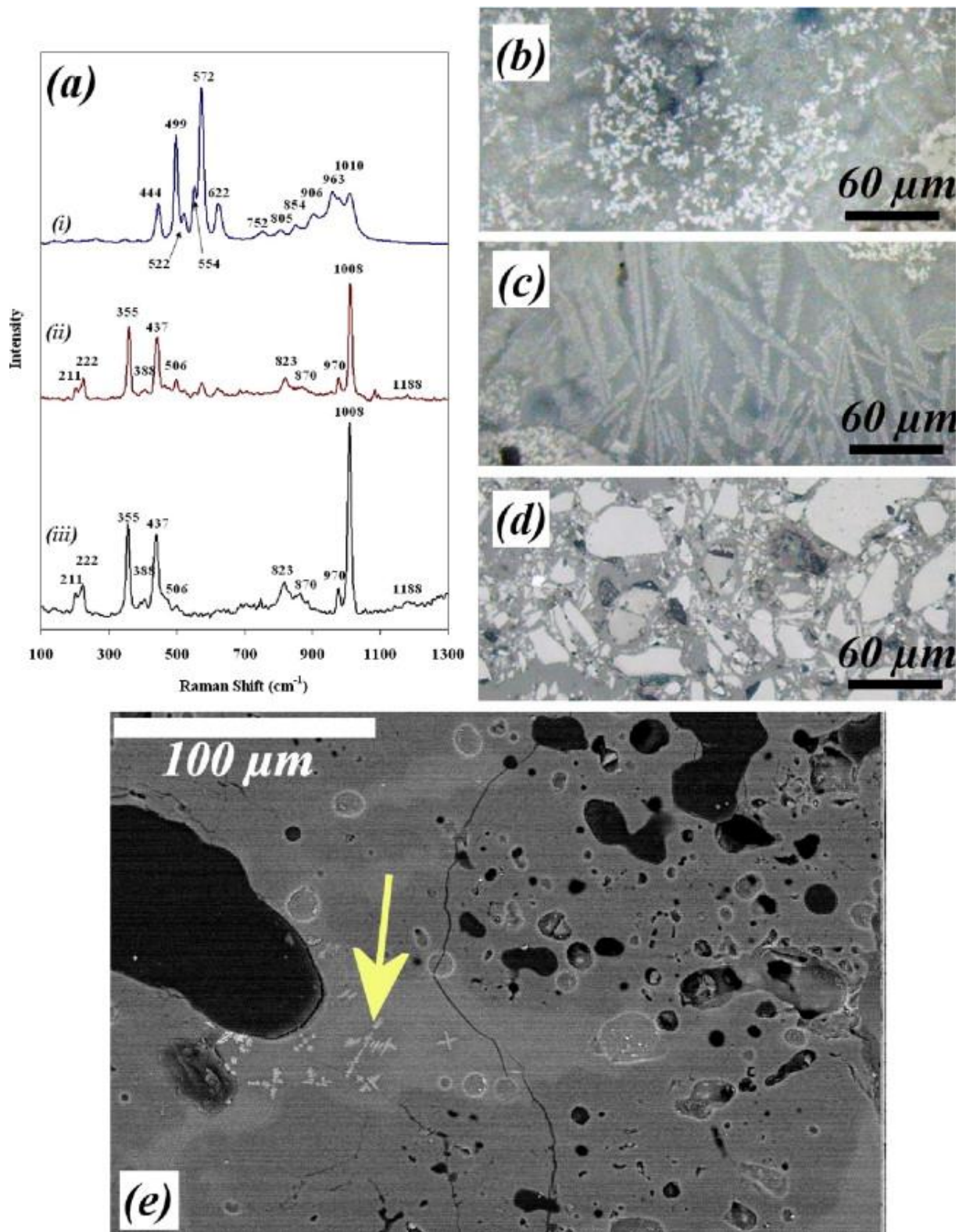
Fig. 10. (a) Raman spectra of the cement showing the transformation of zircon into new phases: (i) spectrum of the small circular grains (b) observed in the fusion crust (distance from exposed surface 1 mm), (ii) spectrum of the dendritic structures (c) observed near the fusion crust (distance from exposed surface 1.5 mm) and (iii) spectrum of the well preserved zircon particles (d) at the back of the sample (distance from exposed surface 8 mm). (e) SEM image showing the intermixing of the fused Mg-rich cement (lighter coloured areas with dendritic

crystals of zircon, arrow) and chert fragments in the fusion crust (un-etched surface, distance from the exposed surface 0.8 mm). Note the bubbles of trapped air.

Zircon crystals in the cement are well preserved below the fusion crust (up to 2 mm from the surface) (Fig. 10d) but adjacent to the fusion crust (between 0.8 mm and 2 mm) the mineral occurs in three forms: as well preserved crystals, as aggregates of tiny (≈1 μm) spherical crystals (Fig. 10c), and as dendritic zircon crystals (Fig. 10b). The tiny spherical crystals are associated with a new mineralogical phase that could not be identified by Raman spectroscopy (Fig. 10a). Electron microprobe analyses show that it contains zircon and magnesium oxide. The distinct change in the morphology, and size of the crystals in the fusion crust (Fig. 10), indicates that temperatures exceeded the maximum service temperature of the cement (1426 °C, manufacturer's data).

3.4. Microfossils

3.4.1. Pre-flight sample

Fossilised microbial cells in the form of colonies of coccoids, chains of coccoids, filaments and associated EPS were identified by HR-SEM microscopy in the original rock (Fig. 11a and b) (cf. Westall et al., 2006). The fossil cells are individually too small (<1 μm) to be distinguished in the fine grained chert matrix by optical microscopy. HR-SEM documented the close relationship between the fossilised colonies of coccoids and the volcanic protoliths (Westall et al., 2006, Fig. 11a and b). Optical microscopy shows that aggregates of dark spots are commonly associated with the volcanic protoliths and Raman spectroscopy confirmed their carbonaceous composition (Fig. 12). Orberger et al. (2006) also noted a close association between carbon and the surfaces of the volcanic protoliths. D and G peak intensities in the Raman spectra of the spots of carbon in the aggregates indicate that the kerogen has a maturity that is consistent with the low grade metamorphism experienced by rocks in the region (prehnite–pumpellyite to lowermost greenschist). We interpret the aggregates observed by optical microscopy in thin section to be the same colonies of coccoids observed by HR-SEM.
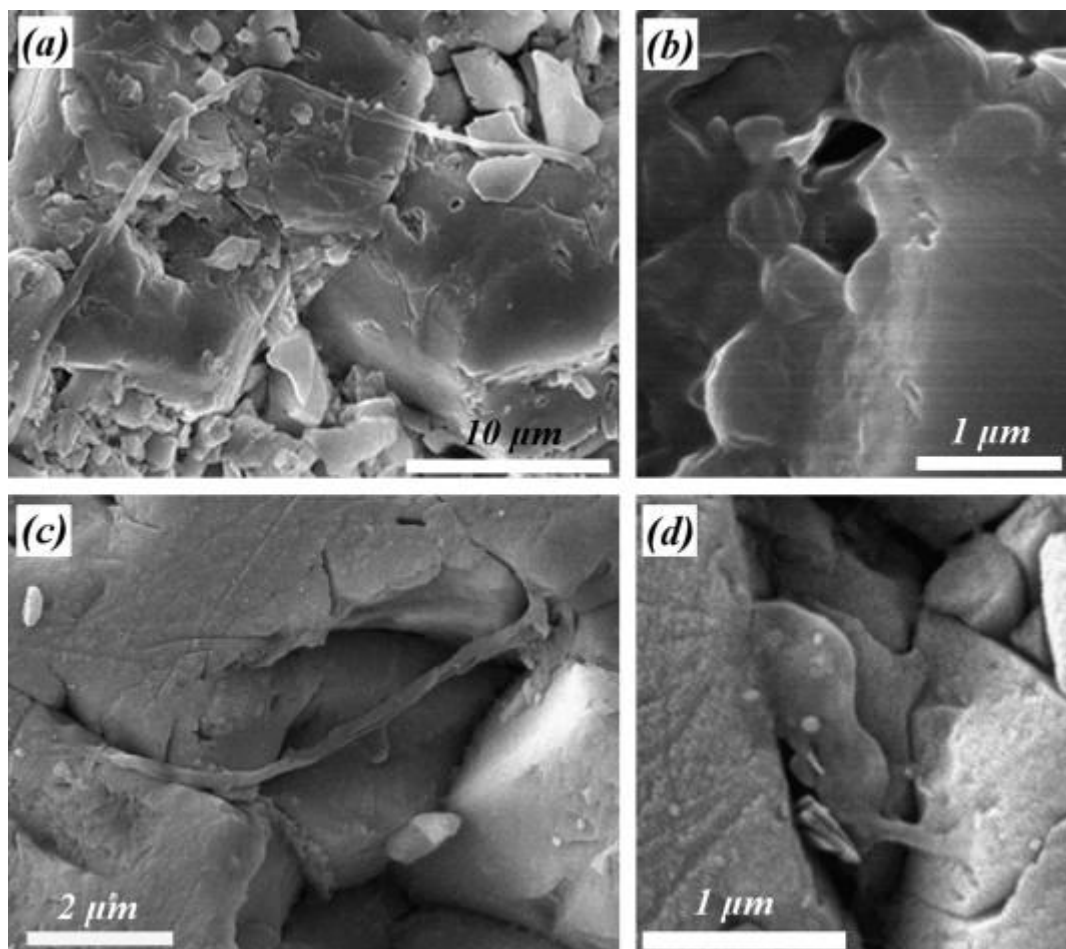
Fig. 11. Comparison between (a) pre-flight and (b) post-flight microfossils. (a and c) Filaments (distance from exposed surface 7.3 mm) and (b and d) coccoid structures (distance from exposed surface 7.2 mm).

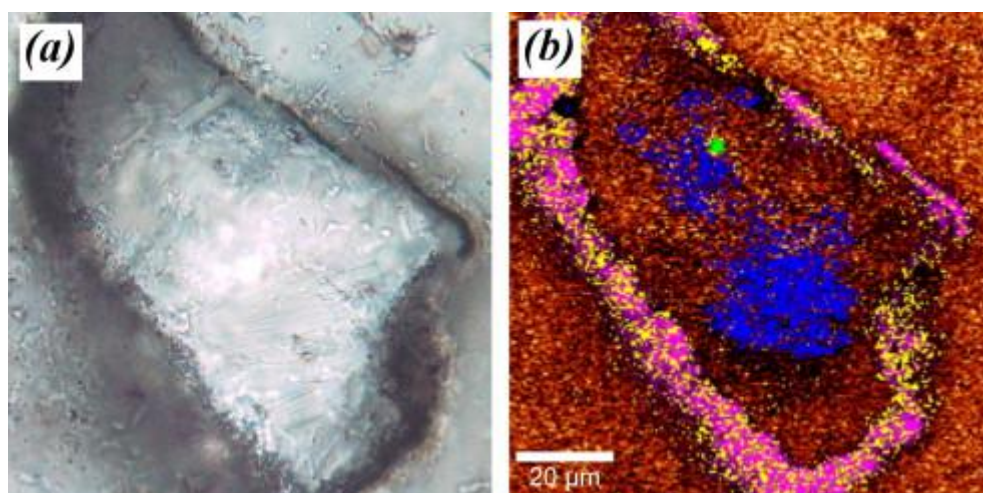Fig. 12. (a) Optical and (b) Raman analysis of organic matter on the surface of a hydromuscovite grain. The Raman image clearly shows the distribution of anatase and carbon around the grain (colour encoding: carbon in yellow, anatase in pink, quartz in brown, muscovite in blue and rutile in green). (For interpretation of the references to colour in this figure legend, the reader is referred to the web version of this article.)

3.4.2. Post-flight sample

HR-SEM observation of un-etched and etched surfaces of thin sections of the flown samples document the presence of a variety of carbonaceous structures including aggregates of tiny carbonaceous spots (Fig. 13 and Fig. 14), coccoidal structures, filaments and EPS (Fig. 11 and Fig. 13), interpreted to be the same types of microfossils described by Westall et al. (2006) in a sawn, etched surface of the Kitty's Gap Chert. The Raman analyses of large aggregates of spots of carbonaceous matter demonstrated the maturation of the kerogen towards the fusion crust (see Fig. 15).

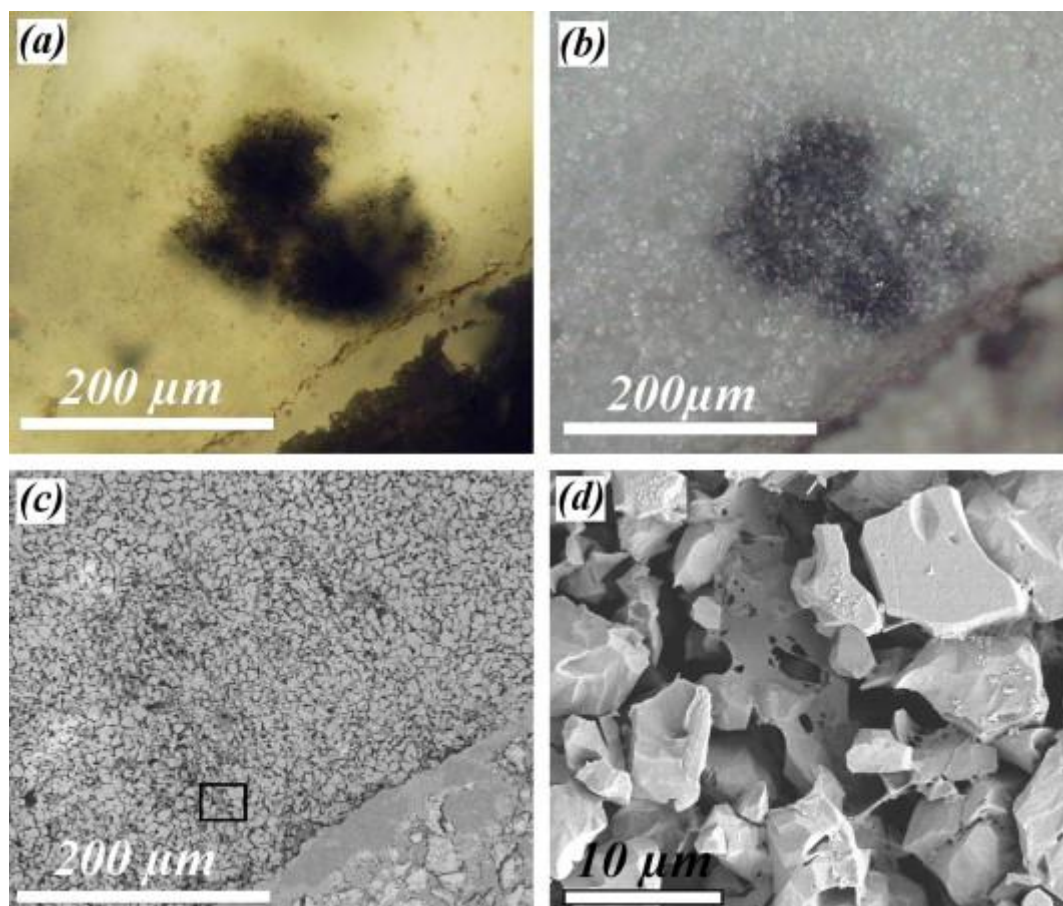Fig. 13. (a) Optical transmitted light image of spots of organic matter forming a dark aggregate (probably a fossilised colony of microorganisms, cf. Westall et al., 2006) in the chert matrix. (b) Same area after HF etching (24%, 45 min). (c) SEM image of the same area and (d) HR-SEM image of the aggregate (in black in (c)) showing a thick film of silicified EPS (distance from the exposed surface 5.5 mm).
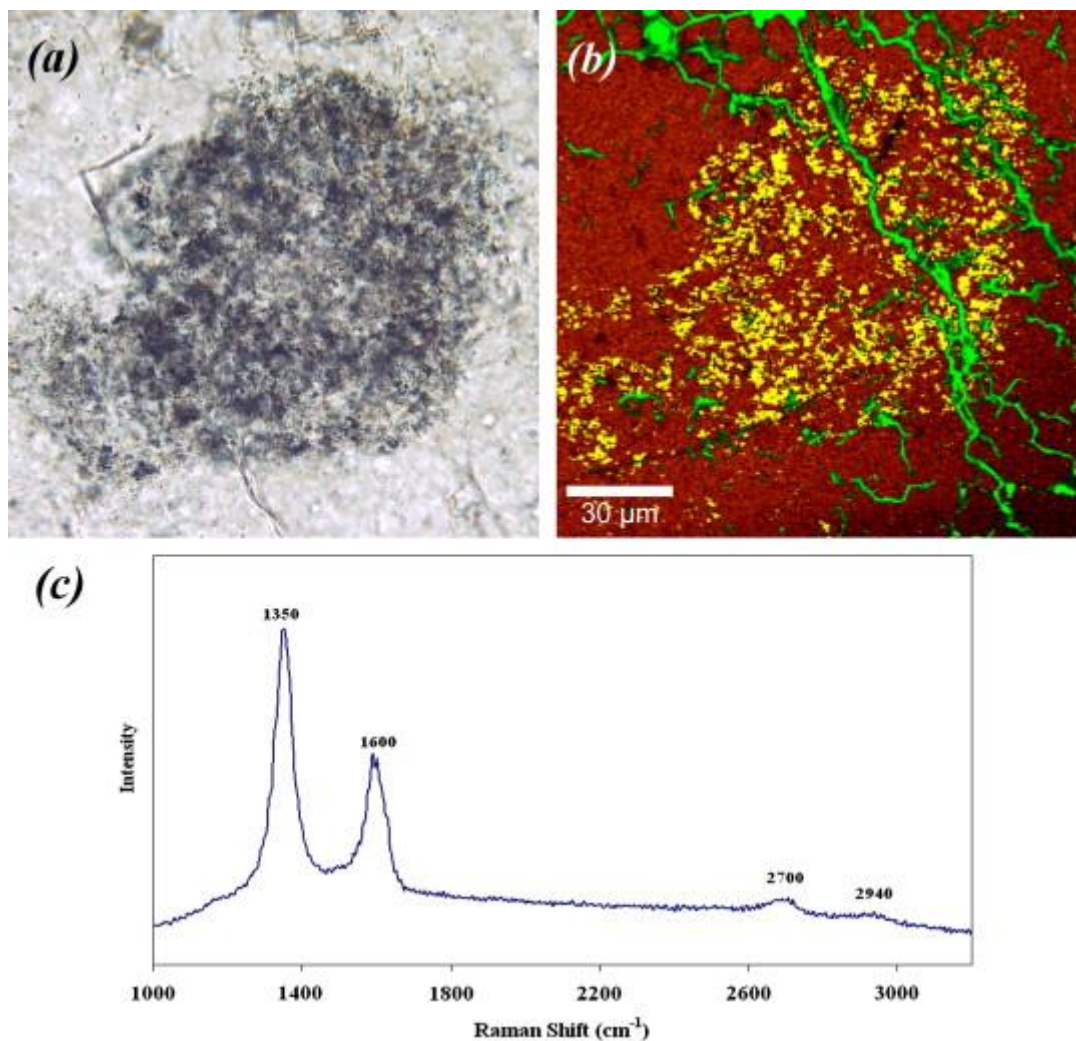
Fig. 14. (a) Optical and (b) Raman image of a dark carbonaceous aggregate (distance from exposed surface 6.0 mm). The Raman image associated with the optical image clearly shows the carbonaceous nature of the spots (in yellow in the figure, corresponding to the 1350 cm^{-1} peak). The presence of cracks in the quartz is enhanced by fluorescence in the image (green in the figure). The intensity of the disorder peak of carbon at 1350 cm^{-1} is significantly higher than the intensity of the graphite peak at 1600 cm^{-1}. The second-order of carbon peaks located at 2700 and 2940 cm^{-1} are also shown (colour encoding: quartz in brown, carbon in yellow and fluorescence in green).
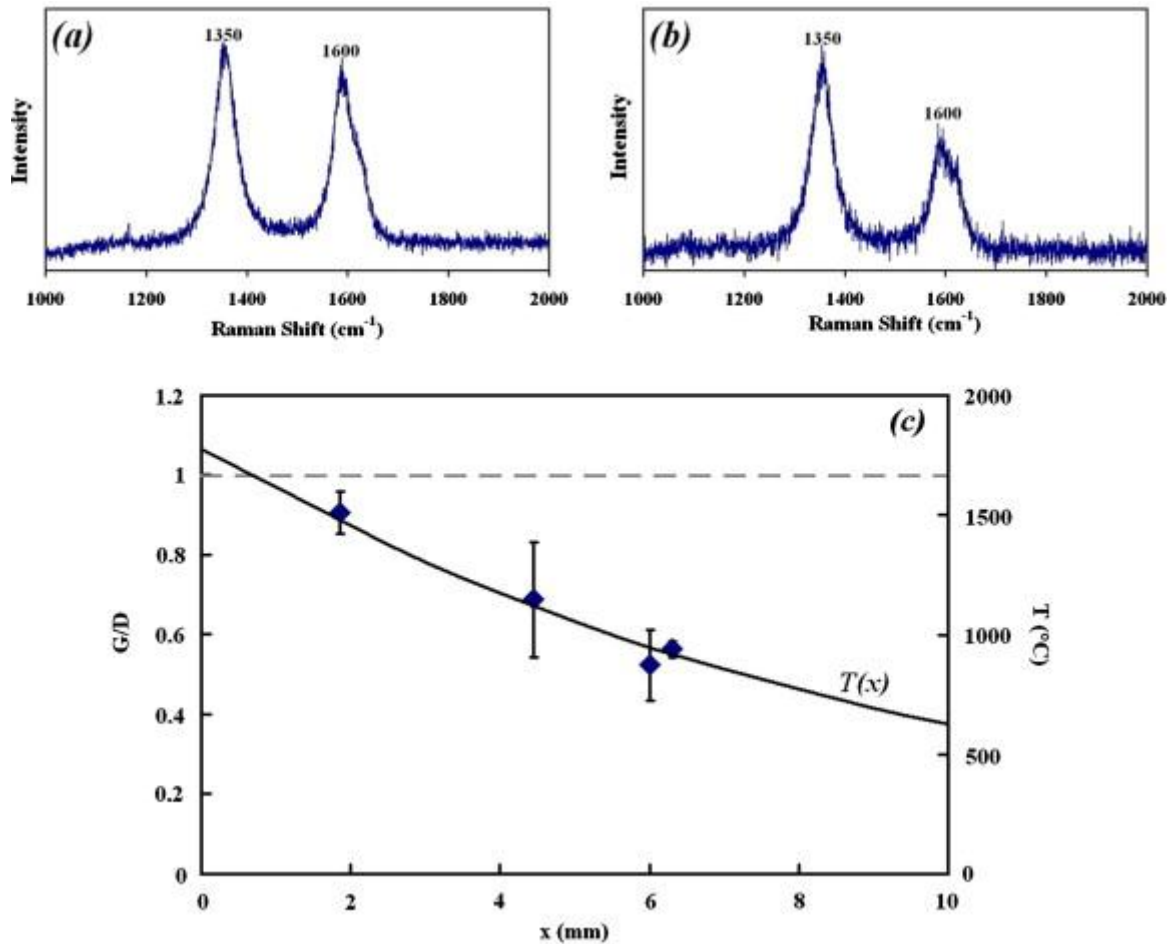
Fig. 15. Raman spectra associated with large aggregates of spots of carbonaceous matter (a) near the fusion crust (distance from the exposed surface 2 mm) and (b) at the back of the sample (distance from the exposed surface 6.2 mm). (c) Ratio of the graphite (*G*) and disorder Raman (*D*) peak intensities versus distance from the exposed surface (*x*).

Our observations of thin section surfaces brought to light another type of carbonaceous structure associated with the volcanic protolith surfaces. Some of the protoliths exhibit tunnel-like cavities at their edges (Fig. 16a) filled with smooth, globular or filamentous filmy carbonaceous matter (Fig. 16b–d), probably representing microbial corrosion pits filled with EPS and the degradation products of chemolithotrophic microorganisms (cf. Furnes et al., 2004 and Banerjee et al., 2007).
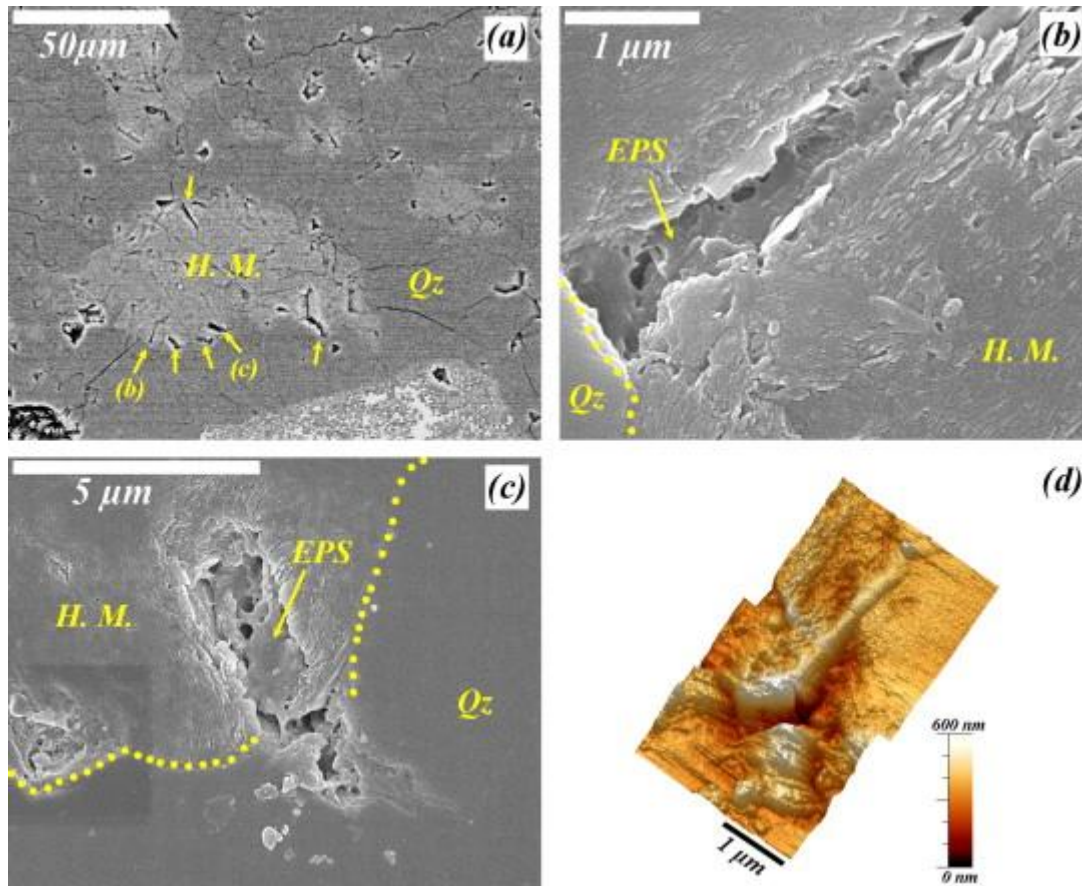
Fig. 16. (a) SEM image showing tunnel structures (arrows) located around a hydromuscovite (H. M.) grain (distance from the fusion crust 9.8 mm). (b and c) HR-SEM images of the tunnel structures located in (a). A thick film of silicified EPS has filled the tunnels (arrows). Filamentous structure observed in the tunnel (c) is shown by AFM in (d) (80×80 μm^2 in size, AFM image processing using *WSxM*, Horcas et al., 2007).

3.5. Modern *Chroococcidiopsis* biofilm

The back of the sample was inoculated with a live culture of *Chroococcidiopsis* microorganisms using a brush. These ≈5 μm sized photosynthetic microorganisms (Fig. 17a) occur naturally as endolithic organisms within cracks in rock surfaces (Cockell et al., 2007).

Fig. 17. (a) Optical view of *Chroococcidiopsis* bacteria. (b) HR-SEM image of the carbonised bacteria at the back of the sample after the experiment.

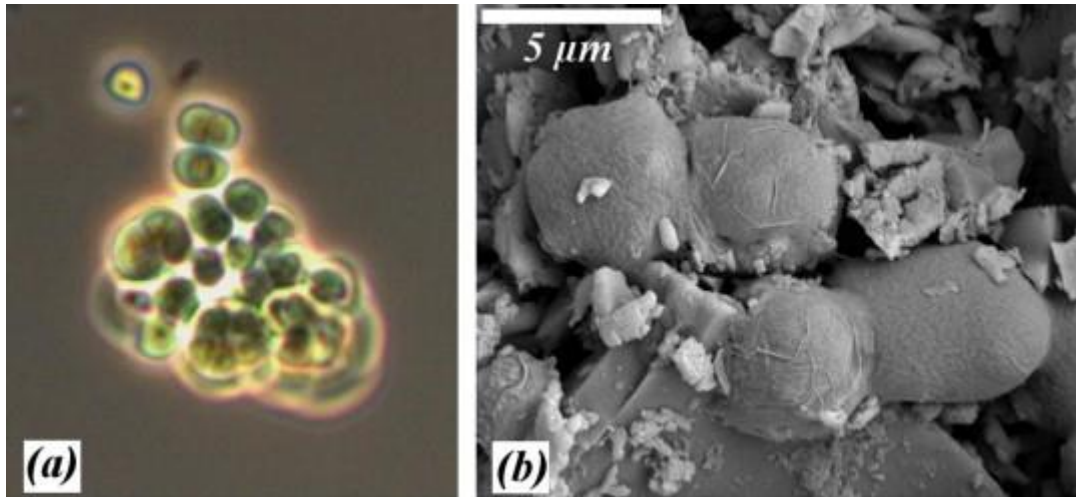No live microorganisms were found on the back of the flown rock. HR-SEM revealed carbonaceous oval cell-like structures occurring either singly (Fig. 17b), or attached to each other in apparent cell division, associated with a carbonaceous film. These structures have a limited size range from 4 to 5 μm. Given their carbonaceous composition and morphological similarity with the original microorganisms, we believe that they represent the carbonised remains of *Chroococcidiopsis*. Had the carbonaceous spheroids been produced simply from the soot of the burnt organisms, they would not exhibit the regularity of size and shape that is characteristic of these microorganisms. Raman analysis of the burnt carbon showed *D* and *G* band components characteristic of trigonal and tetrahedral carbon bonding structures, referred to as the graphite and diamond structural types.

4. Discussion

4.1. Mineralogical changes

Mineralogical changes observed in the flown Kitty's Gap Chert include (1) melting of quartz (1723 °C, Shchipalov, 2002), hydromuscovite (1320 °C) and cement (1426 °C, manufacturer's data) in the fusion crust, (2) the change in quartz phase from α quartz into β quartz at 573 °C (Mosbah et al., 1997), (3) an increase in the size of fluid inclusions in the chert, and (4) the devolatilization of the hydromuscovite (250 °C, Threadgold, 1959). The change in phase from α to β is accompanied by a corresponding change in crystal lattice size (from $a = b = 4.913$ Å, $c = 5.405$ Å for the α quartz and $a = b = 4.9977$ Å and $c = 5.4601$ Å for the β quartz; Mosbah et al., 1997). Rapid quenching of the rock brings about a retrograde phase change back to α quartz and another change in lattice dimension. The dilatation and relaxation of the lattice are probably the causes of the fractures observed in the quartz.

In order to determine the thermal diffusion experienced during atmospheric entry throughout the Kitty's Gap Chert sample, we constructed a new model based on the previous models used by Brandstätter et al., 2008 and Parnell et al., 2008. The details of our model are explained in Appendix A. The model was calibrated using the quartz melting temperature of 1723 °C (Fig. 6) which allowed us to determine that the temperature of the exposed surface was 1775 °C. Since the rock particles are embedded in cement, the thermal diffusivity of the cement was used in the model to estimate the temperatures within the sample. Since diffusivity in the

cement is lower than in the chert, the curves plotted in Fig. 19 correspond to minimal calculated temperatures. They show that the estimated minimal temperature at the back of the sample is 630 °C.

The white colour of the fusion crust may be related more to the fusion of the space cement than to that of the embedded chert fragments. The dark colour of the cement in the lower part of the sample is similar to that noted by Brandstätter et al. (2008) for the carbonate cement of the sandstone in the STONE 5 experiment, which was attributed to thermal alteration. As in the STONE 5 experiment, it appears that flames and heat penetrated behind the sample holder through gaps between the carbon screws and the siliceous sample holder. However, the phase changes observed within the sample show that alteration due to heat from the trailing side was not a significant contribution. This explains the good correlation between the analytical model and the observations.

4.2. Survival of microfossils

Fig. 11 is a comparison of pre-flight and post-flight microstructures (from Westall et al. (2006)) showing that both the filamentous and the coccoid structures are well preserved in the flown rock. The ratio of the graphite (*G*) and disorder (*D*) peak intensity (*G/D*) is plotted versus the distance from the exposed surface in Fig. 15. The *G/D* ratio increases with temperature increase and decreasing distance from the fusion crust, thus demonstrating thermal maturation of the kerogen during atmospheric entry. Graphitization occurs typically at a temperature of about 900 °C, depending on pressure conditions (Bustin et al., 1995). In conclusion, in spite of the mineralogical alteration during atmospheric entry and the maturation of the kerogen, the silicified microorganisms and EPS in the un-melted part of the sample were physically well preserved. We conclude that microfossils from Mars (if martian life existed) could be found in martian sedimentary meteorites.

4.3. Panspermia

Despite the fact that flames may have penetrated to the back of the rock and burnt the *Chroococcidiopsis* biofilm, mineralogical transformations due to the transfer of heat from the surface of the rock indicate that temperatures at the back of the sample were about 630 °C (Fig. 20). This is too high for survival of living microorganisms. Thus even without flames reaching the back of the sample, the 2 cm of rock protection would not have been sufficient to protect endolithic microorganisms. At the surface of the Earth, photosynthetic endoliths, such as *Chroococcidiopsis*, need to have minimum access to light and therefore never penetrate at depths greater than ≈5 mm into the rock. These results are thus in agreement with the conclusion of Cockell et al. (2007) that it is unlikely that photosynthetic organisms can survive transport between planets and, thus, that photosynthesis must have appeared independently on Earth.

What about chemo(litho)trophic organisms? Lithotrophic microorganisms are not dependent on light, obtaining their carbon and energy from inorganic sources. They are common colonisers of rocks and have been found at great depths in deep mines, such as the 3 km deep gold mines of South Africa (Lin et al., 2006). Knowing that rocks ejected during impact can originate from some depth in the crust (⩽100 m, Melosh, 1994 and Melosh, 2003), it is possible that rocks containing lithotrophic microorganisms in their fractures could be ejected by impact. Indeed, if life is still present on Mars, it will occur in protected subsurface environments (McKay et al., 1992). Horneck et al. (2001) have shown that microbial spores

can resist space conditions when protected by a rock/mineral coating but resistance of the living microorganisms to atmospheric entry had not been tested until the STONE 5 and 6 experiments.

The heat flux model (Appendix A, Fig. 19) can be used to determine the minimal thickness of rock necessary to ensure the survival of living organisms. Using the thermal diffusivity of the basalt, the most common rock type that could contain endolithic organisms ($\kappa_{basalt} = 8 \times 10^{-7}$ m^2 s^{-1}), the maximal temperature reached within the sample has been plotted in Fig. 20. It is shown that the thickness needs to be higher than $\approx$5 cm in order to keep a maximal temperature at the bottom of the meteorite that does not exceed 113 °C, the maximal temperature for (hyperthermophilic) life. However, it is worth noting that this model is based on the heating profile experienced by the FOTON capsule. In the case of true meteorites it has been shown that the velocity is higher in such a way that the temperatures generated by frictional heating will be higher but will last less time (Parnell et al., 2008). As a consequence, the temperature reached within the rock will be probably lower than the estimated one in the STONE 6 experiment. The increase of temperature at the surface will be associated with higher ablation of matter but this effect will be counterbalanced by the rotation of the meteorites and by a decrease in the heating time. The quantity of matter ablated during this experiment can thus be considered to be relatively similar to that for true meteorites.

It should be noted that, although the Mars analogue sediment and its microfossils survived the thermal shock of atmospheric entry this experiment does not show if they could have survived the mechanical pressures exerted during the ejection of rocks from Mars. The martian meteorites show moderate levels of shock, typically about 30 GPa (Head et al., 2002). Temperatures can be up to 10,000 °C near the impact point leading to vaporization of the rock, but are typically between 500 and 3000 °C for the surrounding rock. Table 1 compares the compressive strengths of a variety of naturally occurring lithologies. These values provide some indication of the resistance of different rock types to pressure, thus providing an approximation of their reaction to impact pressure. Chert has a higher compressive strength (>250 MPa) than limestone (50–100 MPa) or highly weathered rock (1–5 MPa). Because of their compactness, the silicified volcanic sediments from the 3.446-Ga-old Kitty's Gap better resist these temperatures than less consolidated porous materials (Stöffler, 1984 and French, 1998). Moreover, despite the intense effects of impacts on the country rock, Melosh (1985) determined that intact rock fragments can be ejected from planetary surfaces without suffering too much petrological damage if they were protected by stress wave interference close to the free surface. Indeed, the existence of intact (but shocked) volcanic rocks from Mars is testimony to this process. O'Keefe and Ahrens (1985) calculated that rock fragments about 22 m in diameter could be launched to escape velocity from a 50-km crater on Mars.

Table 1. Comparison of the compressive strengths of different rock types (after Brown (1981)).

Rock type	Uniaxial compressive strength (MPa)
Fresh basalt, chert, diabase, gneiss, granite, quartzite	>250
Amphibolite, sandstone, basalt, gabbro, gneiss, granodiorite, peridotite, rhyolite, tuff	100–250
Limestone, marble, sandstone, schist	50–100
Phyllite, schist, siltstone	25–50
Chalk, claystone, potash, marl, siltstone, shale, rocksalt	2–25
Highly weathered or altered rock, shale	1–5

5. Conclusion

The objectives of the STONE 6 experiment were to determine the effects of thermal alteration during atmospheric entry of martian analogue sediments and the survival of extant and fossil microorganisms during atmospheric entry. The admixture of fragments of ≈3.5 Ga old, silicified volcanic sediments and space cement survived the thermal shock well, forming a white fusion crust. This contrasts strongly with the black crust typical of basaltic martian meteorites (although the colour of the fused material in our experiment may be an artefact of the space cement mixture).

A number of critical mineralogical phase changes and alterations occurred in the chert fragments at different depths in the thickness of the flown rock, including melting of the quartz and hydromuscovite, transition of quartz into quartz β and back to quartz α, and degassing of OH in the hydromuscovite. The evolution of the temperature within the sample could be thus modelled, showing that the maximum temperature reached at the surface of the sample was 1775 °C and at the back of the sample it was ≈630 °C.

Microfossils embedded in the chert fragments survived structurally, except in the fusion crust and only a slight maturation of the kerogen was observed. By analogy, it is concluded that microfossils dating back from the Noachian period could also survive the atmospheric entry and that they could be found in martian sedimentary meteorites, assuming survival during the initial impact leading to ejection. Although our model of the thermal gradient within the sample shows that 2 cm of rock thickness would not be sufficient to protect live microorganisms from the high temperatures experienced at the back of the sample, it may still be possible for endolithic lithotrophs in martian crustal rocks to survive ejection, space transport and atmospheric entry in larger meteorites.

Acknowledgments

Appendix A.

A.1. Modelling temperature distribution

We constructed an analytical model in order to determine the evolution of the temperature within the sample during atmospheric entry. Previously Kimura et al. (2003) and Parnell et al. (2008) used a Heviside step function (i.e. $T(t) = 0$ for $t < 0$, $T(t) = T_{max}$ for $0 < t < \tau$ and $T(t) = 0$ for $t > \tau$) to model the thermal conditions undergone by meteorites. This model is associated with very rapid heating, temperature retention for a short period of time and then very rapid cooling. However, the experimental data of the heat stream measured on the capsule shows that heating, and thus the temperature, at the surface of the sample was progressive (Fig. 18). In order to take this evolution into account as well as possible in the model, the curve was decomposed into several sections of constant temperature (Fig. 18). Adopting an initial temperature of 0 °C, which is approximately the temperature at the top of the stratosphere (stratopause), the temperature at the heating surface at the time t is thus given by:

$$
T(0,t) = \begin{cases}
T_0, & \text{for } t \leqslant \tau_0 \\
T_1, & \text{for } \tau_0 < t \leqslant \tau_1 \\
\vdots & \\
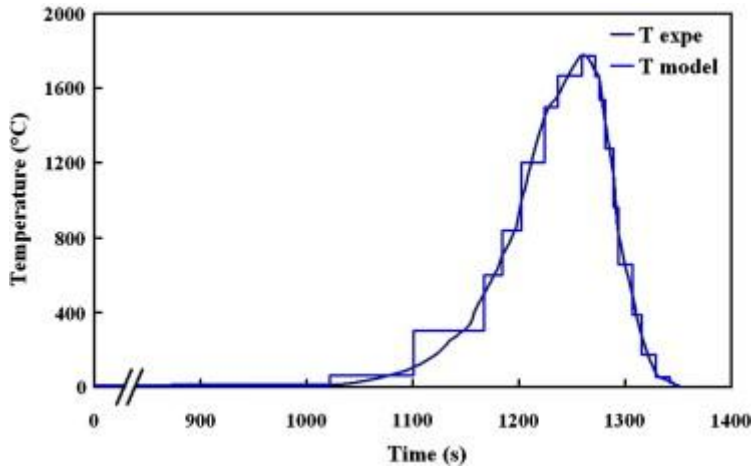T_n, & \text{for } \tau_{n-1} < t \leqslant \tau_n.
\end{cases}
$$

Fig. 18. Variation in temperature at the exposed surface of the flown sample during entry into the Earth's atmosphere as a function of heating time. The "stairs" curve used for the model have been reported.

The global function $T(x, t)$ is thus expressed for each step n as $T_n(x, t)$. Time evolution of the temperature distribution can be obtained by solving the following diffusion equation:

$$
\frac{\partial T}{\partial t} = \kappa \frac{\partial^2 T}{\partial x^2},
$$

where κ is the thermal diffusivity of the material. Since the sample is initially in thermal equilibrium, for the first step the solution is given by:

T0(x,t)=T0.

Mathematical induction can be used to prove that the statement

$$T_n(x,t) = T_{n-1}(x,t) + (T_n - T_{n-1})\left(1 - \mathrm{erf}\,\frac{x}{\sqrt{4\kappa(t - \tau_{n-1})}}\right)$$

holds for all natural numbers n, with erf the error function given by:

$$\mathrm{erf}(z) = \frac{2}{\sqrt{\pi}} \int_0^z e^{-\zeta^2} d\zeta,$$

Thus:

$$\frac{\mathrm{erf}(z)}{dz} = \frac{2}{\sqrt{\pi}} e^{-z^2}.$$

It is worth noting that for $x = 0$, the condition $T_n(0, t) = T_n$ (Eq. (1)) is satisfied.

A.1.1. Basis

In the following, we define:

$$\chi_n = \frac{x}{\sqrt{4\kappa(t - \tau_{n-1})}}$$

And thus:

$$\frac{\partial \chi_n}{\partial x} = \frac{1}{\sqrt{4\kappa(t - \tau_{n-1})}},$$

$$\frac{\partial \chi_n}{\partial t} = -\frac{x}{2(t - \tau_{i-1})\sqrt{4\kappa(t - \tau_{n-1})}}.$$

For $n = 1$:
(10)
$T_1(\chi_1)=T_0+(T_1-T_0)(1-\mathrm{erf}\chi_1).$

This leads to:

$$\frac{\partial T_1(x, t)}{\partial t} = (T_1 - T_0)\frac{2}{\sqrt{\pi}} e^{-\chi_1^2} \frac{\chi_1}{2(t - \tau_0)},$$

$$\frac{\partial^2 T_1(x,t)}{\partial x^2} = (T_1 - T_0)\frac{2}{\sqrt{\pi}}e^{-\chi_1^2}\frac{\chi_1}{2\kappa(t-\tau_0)}.$$

The two sides of the diffusion equation (Eq. (2)) are thus equal for $n = 1$, so the statement (Eq. (4)) is true for $n = 1$. Thus it has been shown that $T_1(x, t)$ holds.

A.1.2. Inductive step

Assuming $T_n(x, t)$ holds, it must be shown that then $T_{n+1}(x, t)$ holds, that is:

$$T_{n+1}(x,t) = T_n(x,t) + (T_{n+1} - T_n)\left(1 - \mathrm{erf}\frac{x}{\sqrt{4\kappa(t-\tau_n)}}\right).$$

The two parts of Eq. (2) are given by:

$$\frac{\partial T_{n+1}(x,t)}{\partial t} = \frac{\partial T_n(x,t)}{\partial t} + (T_{n+1} - T_n)\frac{2}{\sqrt{\pi}}e^{-\chi_{n+1}^2}\frac{\chi_{n+1}}{2(t-\tau_n)},$$

$$\frac{\partial^2 T_{n+1}(x,t)}{\partial x^2} = \frac{\partial^2 T_n(x,t)}{\partial x^2} + (T_{n+1} - T_n)\frac{2}{\sqrt{\pi}}e^{-\chi_{n+1}^2}\frac{\chi_{n+1}}{2\kappa(t-\tau_n)}.$$

Since

$$\frac{\partial T_n(x,t)}{\partial t} = \kappa\frac{\partial^2 T_n(x,t)}{\partial x^2},$$

it is deduced that

$$\frac{\partial T_{n+1}(x,t)}{\partial t} = \kappa\frac{\partial^2 T_{n+1}(x,t)}{\partial x^2},$$

therefore $T_{n+1}(x, t)$ holds.

Since both the basis and the inductive step have been proved, it has now been proved Eq. (4) is solution for all natural n.

A.2. Numerical application

In order to fit the "stairs" curve used in the model (Fig. 18), a well known temperature is needed. The observations show that the quartz particles located at the exposed surface melted in the first ≈ 0.8 mm (Fig. 6); the temperature reached at this depth is thus equal to the melting point of quartz, i.e. 1723 °C (Shchipalov, 2002). Using the thermal diffusivity of the quartz $(\kappa_{Qz} = 5 \times 10^{-6}$ m^2 s$^{-1})$, Eq. (4) leads to the maximum temperature reached at the surface: 1775 °C. This temperature is then used as a reference to estimate the temperature deeper within the sample.

Since the rock particles are embedded in the cement, the thermal diffusivity of the cement ($\kappa_{cement} = 6 \times 10^{-7}$ m^2 s^{-1}) is used to determine the temperature distribution within the sample. Since the cement is the least diffusive component, the temperatures obtained in the model therefore correspond to minimal values.

The temperature versus time is plotted for various depths in Fig. 19. The curves have been smoothed in order to erase the stepped aspect associated with the model. The following relevant mineral alteration temperatures have been added to Fig. 19 in order to compare the model with the experimental observations:

$T_f^{quartz} = 1723\,°C$, the melting point of quartz (Shchipalov, 2002),

T^{cement} = 1426 °C, the maximum service temperature of the cement,

$T_f^{muscovite} = 1320\,°C$, the melting point of muscovite,

$T_{ana\to rut}$ = 610 °C, the phase transition temperature of anatase into rutile (Jamieson and Olinger, 1969),

$T_{\alpha\to\beta}^{quartz} = 573\,°C$, the phase transition temperature from α quartz into β quartz (Shchipalov, 2002 and Mosbah et al., 1997),

T^{hydro} = 250 °C, the lower temperature of loss of hydroxyl water in hydromuscovite (Threadgold, 1959).
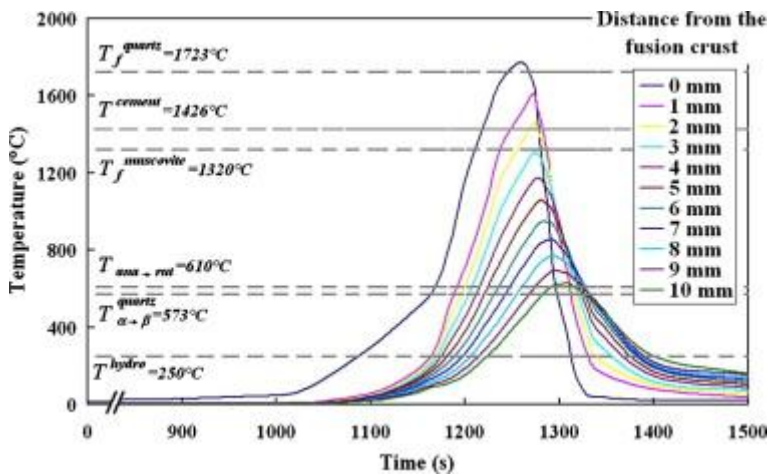

Fig. 19. Temperature distribution as a function of heating time and depth in the sample, after smoothing of the curves. The temperatures of relevant mineral alteration have been added to the figure.
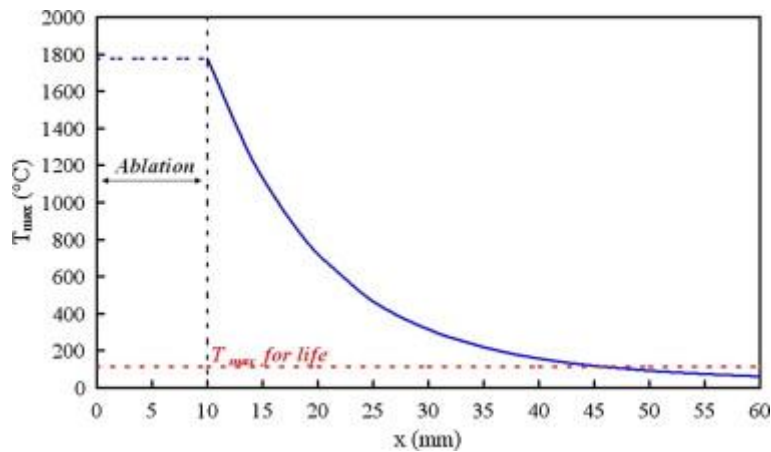
Fig. 20. Maximum temperature versus depth in a basalt sample estimated from the analytical model. The maximal temperature for life has been reported (113 °C).

Thus, according to the model, the quartz melted in the first 0.4 mm, the cement underwent temperatures exceeding the maximum service temperature in the first 2 mm and the muscovite melted in the first 3 mm. Throughout the sample, anatase transformed into rutile, α quartz turned into β quartz and devolatilization occurred in the hydromuscovite. These results are in good accordance with the observed mineral alteration despite the approximation on the thermal diffusivity of the sample.

References

A.C. Allwood, M.R. Walter, B.S. Kamber, C.P. Marshall, I.W. Burch
Stromatolite reef from the Early Archaean era of Australia
Nature, 441 (2006), pp. 714–718

A.C. Allwood, J.P. Grotzinger, A.H. Knoll, I.W. Burch, M.S. Anderson, M.L. Coleman, I. Kanik
Controls on development and diversity of Early Archean stromatolites
Proc. Natl. Acad. Sci. USA, 106 (2009), pp. 9548–9555

N.R. Banerjee, A. Simonetti, H. Furnes, H. Staudigel, K. Muehlenbachs, L. Heaman, M.J. Van Kranendonk
Direct dating of Archean microbial ichnofossils
Geology, 35 (2007), pp. 487–490

Bibring, J.-P., 10 colleagues, and the OMEGA Team, 2005. Mars surface diversity as revealed by the OMEGA/Mars Express observations. Science 307, 1576–1581.

Bishop, J.L., and 11 colleagues, 2008. Phyllosilicate diversity and past aqueous activity revealed at Mawrth Vallis, Mars. Science 321, 830–833.

J. Blichert-Toft, F. Albarède, M. Rosing, R. Frei, B. Bridgwater
The Nd and Hf isotopic evolution of the mantle through the Archean. Results from the Isua supracrustals, West Greenland, and from the Birimian terranes of West Africa
Geochim. Cosmochim. Acta, 63 (1999), pp. 3901–3914
A. Brack

Why exobiology on Mars?
Planet. Space Sci., 44 (1996), pp. 1435–1440

A. Brack
Life on Mars: A clue to life on Earth?
Chem. Biol., 4 (1997), pp. 9–12

Brack, A., and 11 colleagues, 1999. An integrated exobiology package for the search for life on Mars. Adv. Space Res. 23, 301–308.

Brack, A., and 11 colleagues, 2002. Do meteoroids of sedimentary origin survive terrestrial atmosphericentry? The ESA artificial meteorite experiment STONE. Planet. Space Sci. 50, 763–772.

Brandstätter, F., and 10 colleagues, 2008. Mineralogical alteration of artificial meteorites during atmospheric entry. The STONE 5 experiment. Planet. Space Sci. 56, 976–984.

T.E. Brown
Rock Characterization, Testing and Monitoring: ISRM Suggested Methods
Pergamon Press, Oxford (1981) pp. 171–183

R.M. Bustin, J.V. Ross, J.N. Rouzaud
Mechanisms of graphite formation from kerogen: Experimental evidence
Int. J. Coal Geol., 28 (1995), pp. 1–36

M.H. Carr
The Surface of Mars
Cambridge University Press, Cambridge (2006) 307 pp

Cockell, C.S., and 14 colleagues, 2007. Interplanetary transfer of photosynthesis: An experimental demonstration of a selective dispersal filter in planetary island biogeography. Astrobiology 7 (1), 27–29.

de la Torre, R., and 17 colleagues, 2010. Likelihood of interplanetary transfer of rock-inhabiting microbial communities: Results from the space experiment *Lithopanspermia*. Icarus, submitted for publication.

S.T. de Vries, W. Nijman, J.R. Wijbrans, D.R. Nelson
Stratigraphic continuity and early deformation of the central part of the Coppin Gap Greenstone Belt, Pilbara, Western Australia
Precambrian Res., 147 (2006), pp. 1–27

C.I. Fassett, J.W. Head III
Valley network-fed, open-basin lakes on Mars: Distribution and implications for Noachian surface and subsurface hydrology
Icarus, 198 (1) (2008), pp. 37–56

C.M. Fedo, M.J. Whitehouse
Metasomatic origin of quartz–pyroxene rock, Akilia, Greenland, and implications for Earth's earliest life
Science, 296 (2002), pp. 1448–1452

B.M. French
Traces of Catastrophe, A Handbook of Shock-metamorphic Effects in Terrestrial Meteorite Impact StructuresLunar and Planetary Institute (1998) 120 pp

H. Furnes, N.R. Banerjee, K. Muehlenbachs, H. Staudigel, M. de Wit
Early life recorded in Archean pillow lavas
Science, 304 (2004), pp. 578–581

J.P. Greenwood, R.E. Blake
Evidence for an acidic ocean on Mars from phosphorus geochemistry of martian soils and rocks
Geology, 34 (11) (2004), pp. 953–956

J.N. Head, H.J. Melosh, B.A. Ivanov
Martian meteorite launch: High-speed ejecta from small craters
Science, 298 (2002), pp. 1752–1756

I. Horcas, R. Fernandez, J.M. Gomez-Rodriguez, J. Colchero, J. Gomez-Herrero, A.M. Baro
WSxM: A software for scanning probe microscopy and a tool for nanotechnology
Rev. Sci. Instrum., 78 (2007), pp. 013705-1–013705-8

G. Horneck, P. Rettberg, G. Reitz, J. Wehner, U. Eschweiler, K. Strauch, C. Panitz, V. Starke, C. Baumstark-Kahn
Protection of bacterial spores in space, a contribution to the discussion on panspermia
Origin Life Evol. Biosp., 31 (2001), pp. 527–547

J.C. Jamieson, B. Olinger
Pressure–temperature studies of anatase, brookite rutile, and $TiO_2(II)$: A discussion
Am. Mineral., 54 (1969), pp. 1477–1481

M. Kimura, M. Chen, Y. Yoshida, A.E. Goresy, E. Ohtani
Back-transformation of high-pressure phases in a shock melt vein of an H-chondrite during atmospheric passage: Implications for the survival of high-pressure phases after decompression
Earth Planet. Sci. Lett., 217 (2003), pp. 141–151

Lin, L.-H., and 13 colleagues, 2006. Long-term sustainability of a high-energy, low-diversity crustal biome. Science 314, 479–482.

C.P. McKay
An approach to searching for life on Mars, Europa, and Enceladus
Space Sci. Rev., 135 (2008), pp. 49–54

C.P. McKay, R.L. Mancinelli, C.R. Stoker, R.A. Wharton Jr.
The possibility of life on Mars during a water-rich past
H.H. Kieffer, B.M. Jakosky, C.W. Snyder, M.S. Matthews (Eds.), Mars, University of Arizona Press, Tucson (1992), pp. 1234–1245

H.J. Melosh

Impact cratering mechanics: Relationship between the shock wave and excavation flow
Icarus, 62 (2) (1985), pp. 339–343

H.J. Melosh
Swapping rocks: Exchange of surface material among the planets
Planet. Rep., 14 (1994), pp. 16–19

H.J. Melosh
Exchange of meteorites (and life?) between stellar systems
Astrobiology, 3 (2003), pp. 207–219

Milliken, R.E., and 11 colleagues, 2008. Opaline silica in young deposits on Mars. Geology 36 (11), 847–850.

S.J. Mojzsis, G. Arrhenius, K.D. McKeegan, T.M. Harrison, A.P. Nutman, C.R.L. Friend
Evidence for life on Earth before 3.800 million years ago
Nature, 384 (1996), pp. 55–59

M. Mosbah, J.-P. Duraud, R. Clocchiatti
Use of the $\alpha \rightarrow \beta$ quartz transition to monitor the temperature increase produced by a proton microbeam
Nucl. Instrum. Methods Phys. Res. B, 130 (1997), pp. 171–175

A.P. Nutman, S.J. Mojzsis, C.R.L. Friend
Recognition of $\geqslant$3850 Ma water-lain sediments in West Greenland and their significance for the Early Archaean Earth
Geochim. Cosmochim. Acta, 61 (12) (1997), pp. 2475–2484

J.D. O'Keefe, T.J. Ahrens
Impact and explosion crater ejecta, fragment size, and velocity
Icarus, 62 (1985), pp. 328–338
B. Orberger, V. Rouchon, F. Westall, S.T. de Vries, D.L. Pinti, C. Wagner, R. Wirth, K. Hashizume
Microfacies and origin of some Archean cherts (Pilbara, Australia)
Geol. Soc. Am., 405 (2006), pp. 133–156 (special paper)

J.J. Papike, J.M. Karner, C.K. Shearer, P.V. Burger
Silicate mineralogy of martian meteorites
Geochim. Cosmochim. Acta, 73 (2009), pp. 7443–7485

J. Parnell, D. Mark, F. Brandstätter
Response of sandstone to atmospheric heating during the STONE 5 experiment: Implications for the palaeofluid record in meteorites
Icarus, 197 (1) (2008), pp. 282–290

Poulet, F., Bibring, J.-P., Mustard, J.F., Gendrin, A., Mangold, N., Langevin, Y., Arvidson, R.E., Gondet, B., Gomez, C., and the Omega Team, 2005. Phyllosilicates on Mars and implications for early martian climate. Nature 438, 623–627.

Renno, N.O., and 22 colleagues, 2009. Physical and thermodynamical evidence for liquid water on Mars. J. Geophys. Res. 113, E00A18. doi:10.1029/2008JE003083 (special issue on Phoenix).

M.T. Rosing
13C-depleted carbon microparticles in >3700-Ma sea-floor sedimentary rocks from West Greenland
Science, 283 (1999), pp. 674–676

M.A. Sephton, O. Botta
Extraterrestrial organic matter and the detection of life
Space Sci. Rev., 135 (2008), pp. 25–35

Yu.K. Shchipalov
Thermodynamic analysis of melting, vitrification, and crystallization in the SiO_2 system, glass and ceramics
Sci. Glass Prod., 59 (3–4) (2002), pp. 115–118

G. Southam, F. Westall
Geology, life and habitability
Treatise Geophys., 10 (12) (2007), pp. 421–437

G. Southam, L.J. Rothschild, F. Westall
The geology and habitability of terrestrial planets: Fundamental requirements for life
Space Sci. Rev., 129 (2007), pp. 7–34

Squyres, S.W., and 49 colleagues, 2004. The Spirit Rover's Athena Science Investigation at Gusev Crater, Mars. Science 305, 794–799.

Squyres, S.W., and 17 colleagues, 2008. Detection of silica-rich deposits on Mars. Science 320 (5879), 1063–1067.

D. Stöffler
Glasses formed by hypervelocity impact
J. Non-Crystall. Solids, 67 (1–3) (1984), pp. 465–502

I.M. Threadgold
A hydromuscovite with the $2M_2$ structure, from Mount Lyell, Tasmania
Am. Mineral., 44 (1959), pp. 488–494

M.M. Tice, D.R. Lowe
Photosynthetic microbial mats in the 3,416-Myr-old ocean
Nature, 431 (2004), pp. 549–552

S.H.J.M. van den Boorn, M.J. van Bergen, W. Nijman, P.Z. Vroon
Dual role of seawater and hydrothermal fluids in Early Archean chert formation: Evidence from silicon isotopes
Geology, 35 (10) (2007), pp. 939–942

M.A. van Zuilen, A. Lepland, G. Arrhenius
Reassessing the evidence for the earliest traces of life
Nature, 418 (2002), pp. 627–630

M.M. Walsh
Evaluation of Early Archean volcaniclastic and volcanic flow rocks as possible
sites for carbonaceous fossil microbes
Astrobiology, 4 (4) (2004), pp. 429–437

N.R. Walter, D.J. des Marais
Preservation of biological information in thermal spring deposits: Developing a
strategy for the search for fossil life on Mars
Icarus, 101 (1993), pp. 129–143

S.J. Wentworth, E.K. Gibson, M.A. Velbel, D.S. McKay
Antarctic Dry Valleys and indigenous weathering in Mars meteorites: Implications
for water and life on Mars
Icarus, 174 (2005), pp. 383–395
F. Westall
Life on the early Earth: A sedimentary view
Science, 308 (2005), pp. 366–367

F. Westall, R.L. Folk
Exogenous carbonaceous microstructures in Early Archaean cherts and BIFs from
the Isua Greenstone Belt: Implications for the search for life in ancient rocks
Precambrian Res., 126 (2003), pp. 313–330

F. Westall, G. Southam
The early record of life
Archean Geodynam. Environ., 164 (2006), pp. 283–304

Westall, F., and 13 colleagues, 2000. An ESA study for the search for life on Mars. Planet.
Space Sci. 48, 181–202.

F. Westall, C.E.J. de Ronde, G. Southam, N. Grassineau, M. Colas, C. Cockell, H. Lammer
Implications of a 3.472–3.333 Gyr-old subaerial microbial mat from the Barberton
greenstone belt, South Africa for the UV environmental conditions on the early
Earth
Philos. Trans. R. Soc. Lond. B, 361 (2006), pp. 1857–1875

Westall, F., and 11 colleagues, 2006. The 3.466 Ga "Kitty's Gap Chert", an Early Archean
microbial ecosystem. Geol. Soc. Am., 405, 105–131 (special paper).